This is a preprint, the final version is subject to change, of the American Mineralogist (MSA)
Cite as Authors (Year) Title. American Mineralogist, in press.
(DOI will not work until issue is live.) DOI: http://dx.doi.org/10.2138/am-2015-4863

Scandium- and REE-rich tourmaline replaced by Sc-rich REE-bearing epidote-group mineral from the mixed (NYF + LCT) Kracovice pegmatite (Moldanubian Zone, Czech Republic)

Renata Čopjaková[1*], Radek Škoda[1], Michaela Vašinová Galiová[2,3], Milan Novák[1], Jan Cempírek[4,5]

[1]Department of Geological Sciences, Faculty of Science, Masaryk University, Kotlářská 2, 611 37 Brno, Czech Republic; copjakova@sci.muni.cz

[2]Department of Chemistry, Faculty of Science, Masaryk University, Kotlářská 2, 611 37 Brno, Czech Republic

[3]Central European Institute of Technology (CEITEC), Masaryk University, Kamenice 5, 625 00 Brno, Czech Republic

[4] Department of Mineralogy, Moravian Museum, Zelný trh 6, Brno 61137, Czech Republic

[5] Department of Earth, Ocean and Atmospheric Sciences, University of British Columbia, 2207 Main Mall, Vancouver, BC V6T 1Z4, Canada

* E-mail: copjakova@sci.muni.cz

ABSTRACT

Primary black thick-prismatic Al-rich schorl to rare fluor-schorl (TurP1) locally overgrown by brownish-green Li-rich fluor-schorl to fluor-elbaite (TurP2) from the Kracovice pegmatite (mixed NYF + LCT signature), was partly replaced by secondary Li-rich fluor-schorl to fluor-elbaite (TurS) plus the assemblage REE-bearing epidote-group mineral + chamosite. Primary Al-rich schorl (TurP1) shows high and variable contents of Sc (33-364 ppm) and Y+REE (40-458 ppm) with steep, LREE-enriched REE pattern. Overgrowing (TurP2) and replacing (TurS) Li-rich fluor-schorl to fluor-elbaite zones are typically depleted in Sc (21-60 ppm) and Y+REE (3-47 ppm) with well-developed tetrad effect in the first (La-Nd) and the second (Sm-Gd) tetrads. Scandium- and REE-rich black tourmaline (TurP1) crystallized earlier from the melt whereas crystallization of primary Li-rich fluor-schorl to fluor-elbaite (TurP2) most likely took place during late magmatic to early hydrothermal conditions. Both the secondary Li-rich fluor-schorl to fluor-elbaite (TurS) and the unusual assemblage of REE-bearing

epidote-group mineral + chamosite are likely coeval products of subsolidus reactions of the magmatic Al-rich schorl (TurP1) with evolved REE-poor, Li,F-rich, alkaline pegmatite-derived fluids. Well crystalline REE-bearing epidote-group mineral (Y+REE = 0.42-0.60 apfu) confirmed by Raman spectroscopy has a steep, LREE-rich chondrite-normalized REE pattern with significant negative Eu anomaly and shows variable and high contents of Sc (≤ 3.3 wt. % Sc_2O_3) and Sn (≤ 1.0 wt. % SnO_2). Substitution $ScAl_{-1}$ and minor vacancy in the octahedral sites are suggested in the REE-bearing epidote-group mineral.

Keywords: schorl, fluor-elbaite, tourmaline replacement, Sc-rich REE-bearing epidote-group mineral, granitic pegmatite, Bohemian Massif

INTRODUCTION

Tourmaline is a frequent minor to accessory mineral in rocks of widely variable composition formed in various geological settings including magmatic, metamorphic, sedimentary and hydrothermal environments. Tourmaline is a characteristic mineral of strongly peraluminous granites and pegmatites where it crystallizes either as a primary phase from melt or as a hydrothermal mineral during late-magmatic stage (Wolf and London 1997; London 2014a). Hydrothermal fluids derived from highly fractionated peraluminous granites and pegmatites are commonly enriched in volatiles such as B, Li and F. Tourmaline has a large stability field in terms of both temperature and pressure (Henry and Dutrow 1996; London 2011) and is quite resistant to weathering (Morton and Halsworth 2007). Nevertheless, tourmaline namely in granitic pegmatites is locally altered by late hydrothermal fluids to various, mostly aluminous minerals (e.g., muscovite, chlorite, pumpellyite-(Al); e.g., Dietrich 1985; Ahn and Buseck 1998; Novák et al. 2013; Prokop et al. 2013). The breakdown of tourmaline and its replacement by various Al-silicates during interaction with hydrothermal and metamorphic fluids also were reported from ore deposits and tourmalinites (Slack and Robinson 1990; Leitch and Turner 1992; Čopjaková et al. 2012).

Rare earth elements (REE) - rich minerals of the epidote group belong either to the allanite or the dollaseite subgroups. They have a general formula $^{A1,2}A_2{}^{M1,2,3}(M^{3+}{}_2M^{2+})_3[T_2O_7][TO_4]^{O4}(O)^{O10}(OH)$ with the site occupancy A1 = Ca, Mn, A2 = REE, Th, U, Ca, Sr, M1 = Al, Fe^{3+}, Mn^{3+}, M2 = Al, M3 = Fe^{2+}, Mg^{2+}, Mn^{2+}, O4 = O^{2-},F^-, O10 = OH^- (Gieré and Sorensen 2004; Armbruster et al. 2006). Minerals of the allanite subgroup are derived from clinozoisite by the substitution $^{A2}REE^{3+} + {}^{M3}M^{2+} \rightarrow {}^{A2}Ca^{2+} + {}^{M3}M^{3+}$. The most common members of the allanite subgroup, allanite-(Ce) and ferriallanite-(Ce), occur in

a solid solution as accessory minerals of metaluminous granitic rocks, carbonatites, metamorphic rocks and skarns. In granitic pegmatites they crystallize during the primary (magmatic) or secondary (metasomatic) stages (Peterson and MacFarlane 1993; Hoshino et al. 2006; Škoda et al. 2006; Škoda et al. 2012). Secondary allanite sometimes occurs as a breakdown product of feldspars, biotite and eudialyte during interaction of hydrothermal fluids with granitoid rocks (Pantó 1975; Ward et al. 1992; Coulson 1997). Nevertheless, the mineral assemblage tourmaline + allanite is very rare in granitic pegmatites and other granitic rocks (Novák et al. 2011a, 2012; Čopjaková et al. 2013a).

In the present study, the assemblage of magmatic Al-rich schorl from the Kracovice pegmatite (Bohemian Massif) which was replaced by the hydrothermal assemblage of REE-bearing epidote-group mineral + chamosite + fluor-elbaite was investigated using EMP, LA-ICP-MS and Raman spectroscopy. Chemical variations of both major and trace (Y+REE, Sc) elements in tourmaline were used for genetic implications and to decipher the tourmaline evolution and replacement process. Moreover, textural relations, compositional trends and substitutions mechanisms in extraordinarily Sc-rich REE-bearing epidote-group mineral replacing tourmaline are discussed.

GEOLOGICAL SETTING AND HOST PEGMATITE

The Moldanubian Zone, a highly metamorphosed core of the Bohemian Massif, represents a crustal (and upper mantle) tectonic collage assembled during the Variscan orogeny and modified by several events of superimposed deformation and high- to low-grade metamorphic re-equilibration at about ~ 340-330 Ma. They are: (i) a HP-HT event in upper amphibolite to granulite facies at $T_{max.}$ ~ 850-900 °C and $P_{max.}$ = 1.2-1.8 MPa, more or less overprinted during a rapid decompression by (ii) a MP-HT event at T ~ 700 °C and P ~ 0.4-0.6 MPa (e.g., Pertoldová et al. 2009), and (iii) LP-HT metamorphic event related to contact envelope of granite plutons.

Extensive Variscan igneous activity shows several distinct stages (see Timmerman 2008 for overview): (i) subduction-related normal and high-K calc-alkaline suites (~ 370-345 Ma), (ii) (ultra-)potassic, Mg-rich quartz syenitic to melagranitic plutons – durbachites (~ 340-335 Ma), (iii) moderately to strongly peraluminous anatectic granites formed as a consequence of the LP-HT metamorphic overprint (331-326 Ma), and (iv) late small plutons of fine-grained I-type granitoids associated with minor diorites (319-300 Ma).

The Moldanubian Zone is characterized by the presence of numerous granitic pegmatites of different origin and mineralogy (Novák et al. 2013). They frequently belong to the rare-element class and exhibit substantial variability in size, textural differentiation, degree of fractionation and mineralogy. The pegmatites range from barren to highly fractionated dikes with LCT (enriched in Li, Cs, Ta; dated at 340-325 Ma, Novák et al. 1998a; Melleton et al. 2012), NYF (enriched in Nb, Y, F; dated at ~ 340-335 Ma) and mixed NYF + LCT geochemical signatures (Novák et al. 2012, 2013) using the current classification schemes (Černý and Ercit 2005; Černý et al. 2012). The Třebíč syenite (durbachite) Pluton (for more details see, e.g., Janoušek and Holub 2007) hosts a population of intragranitic NYF pegmatites ranging in textural-paragenetic and geochemical features from primitive metaluminous allanite-subtype pegmatites with allanite-(Ce), titanite, ilmenite and tourmaline (dravite > schorl), to more evolved, metaluminous to slightly peraluminous euxenite-subtype pegmatites containing tourmaline (schorl), ilmenite, titanite, aeschynite- and euxenite-group minerals, beryl, zircon, tinzenite and herzenbergite (Škoda and Novák 2007; Novák et al. 2011a, 2012, 2013; Čopjaková et al. 2013a).

The Kracovice pegmatite is a symmetrically zoned dike, ~ 1 m thick and 30 m long, cutting a graphitic gneiss ca. 300 m W of the edge of the Třebíč Pluton. It represents the most evolved pegmatite body from the population of dominantly NYF pegmatites related to the Třebíč Pluton (Němec 1990; Novák et al. 1999, 2012; Škoda et al. 2006; Čopjaková et al. 2013a). From the contact inwards, the pegmatite consists of: a narrow zone of a coarse-grained granitic unit (Kfs + Pl + Qz + Bt + Ms + Ttn), a wide graphic unit (Kfs + Qz + Tu ± Bt), which evolves to minor blocky K-feldspar, and an albite unit situated close to a small quartz core in the most differentiated part of the dike. Typical minor-to-accessory minerals include tourmaline, Y,Sc-enriched spessartine, topaz, Li micas (Mn-rich polylithionite, masutomilite), beryl, cassiterite, zircon, niobian rutile, minerals of the columbite-, fergusonite-, and samarskite-groups, *wolframoixiolite*, F-rich hambergite, monazite-(Ce), xenotime-(Y) and an REE-bearing epidote-group mineral (Němec 1990; Novák et al. 1998b, 2012; Čopjaková et al. 2013a). Yttrium- and REE-bearing oxides are almost exclusively associated with garnet in the albite unit. The evident Li enrichment along with the presence of Y,REE-oxides suggests the mixed (NYF + LCT) geochemical signature of the pegmatite (Novák et al. 2012).

Tourmaline is present in several morphological, paragenetic and compositional types (Novák 2000; Čopjaková et al. 2013a). Black to brown prismatic crystals and their aggregates, up to several cm in size, occur in the graphic unit, blocky K-feldspar, albite unit

and in the massive quartz; their composition correspond to Al-rich schorl (Al ≥ 6.57 apfu). Brownish-green to yellowish-green prismatic tourmaline crystals and their aggregates up to 1 cm in size as well as narrow rims around grains of the black tourmaline occur especially in the albite unit. Their composition ranges from minor Mn-rich fluor-schorl to common fluor-elbaite (Novák 2000; Čopjaková et al. 2013a).

ANALYTICAL METHODS

Electron microprobe

The tourmaline and associated minerals were studied using the Cameca SX100 electron microprobe (EMP) at Joint Laboratory of Electron Microscopy and Microanalysis, Department of Geological Sciences, Masaryk University, and Czech Geological Survey, Brno. Their chemical composition was analyzed in wavelength dispersive mode and the accelerating voltage 15 kV. Operating conditions for analyses were as follows: beam currents 10 nA for tourmaline and chlorite and 20 nA for REE-bearing epidote-group mineral, and a spot size ~ 5 μm. The following standards and X-ray *K*α lines were used for tourmaline and chlorite analyses: sanidine (Si, Al, K), albite (Na), olivine (Mg), andradite (Ca, Fe), Mn_2SiO_4 (Mn), anatase (Ti), topaz (F), and ZnO (Zn). The following standards and X-ray lines were used for REE-bearing epidote-group mineral analyses: Na *K*α (albite), K,Al,Si *K*α (sanidine), Ca *K*α (wollastonite), Fe *K*α (andradite), Sc *K*α ($ScVO_4$), Sn *L*α (Sn), La *L*α ($LaPO_4$), Ce *L*α ($CePO_4$), Pr *L*β ($PrPO_4$), Nd *L*β ($NdPO_4$), Sm *L*β ($SmPO_4$), Gd *L*β ($GdPO_4$), Ho *L*α ($HoPO_4$), Dy *L*α ($DyPO_4$), Y *L*α (YAG), U *M*β (U), Th *M*α ($CaTh(PO_4)_2$), Pb *M*α (PbSe), Mg *K*α (olivine), Mn *K*α (Mn_2SiO_4), Ti *K*α (anatase), Cr *K*α (chromite), V *K*β (vanadinite), Zr *L*α (zircon), Sr *L*α ($SrSO_4$), Ba *L*α ($BaSO_4$), P *K*α (fluorapatite), F *K*α (topaz), Cl *K*α (vanadinite). The peak counting times were 10 s for major and 20–120 s for minor elements. With regard to the analysis of fluorine, special care was taken to determine the optimal background positions and to minimize the overlap of the F *K*α peak with the Fe *L*α peak position. The empirically determined correction factor was applied to the coincidence of F *K*α and Ce *M*ζ. Raw data obtained from the electron microprobe (in case of tourmaline supplemented by theoretical B and H contents) were reduced using X-Phi matrix correction procedure (Merlet 1994).

Crystal-chemical formulae of Li-rich tourmaline (TurP2,TurS) were calculated on the basis of Si = 6 assuming the general formula $XY_3Z_6T_6O_{18}(BO_3)_3V_3W$, where X = Na, Ca, K, vacancies; Y = Fe, Mg, Mn, Ti, Al, Zn; Z = Al, Fe, Mg; T = Si; B = B; V + W = OH + F + O = 4 as recommended by Henry et al. (2011) although such approach may overestimate other cations where ^{T}Al is present. Crystal-chemical formulae of Li-poor tourmaline (TurP1,

TurP1c) were calculated on the basis of T+Z+Y site cations = 15, because normalization on the basis of Si = 6 yielded the sum of T+Z+Y cations > 15 which indicated a deficiency of Si at the T-site and presence of ^{T}Al. All Fe is considered as Fe^{2+} although unpublished wet chemical analysis of schorl from Kracovice by P. Povondra yields 2.90 wt. % Fe_2O_3 and 11.02 wt. % FeO. Crystal-chemical formulae of chamosite were obtained on the basis of 18 anions, all Fe is reported as Fe^{2+} and the water content was calculated assuming OH = 8. Formulae of the REE-bearing epidote-group mineral (EGM) were normalized on the basis of 3 Si cations. The water content was calculated assuming the ideal 1 OH occupancy and the Fe^{2+}/Fe^{3+} ratio was calculated to maintain the mineral formula electro-neutral.

Laser Ablation Inductively Coupled Plasma Mass Spectrometry

The LA-ICP-MS at the Department of Chemistry, Masaryk University, Brno, consists of a laser ablation system UP 213 (New Wave Research, Inc., Fremont, CA, USA) and an ICP-MS spectrometer Agilent 7500 CE (Agilent Technologies, Santa Clara, CA, USA). The pulsed (4.2 ns) Nd:YAG laser operates at 213 nm and is equipped with an ablation chamber of the type SuperCell. Aerosol generated in the SuperCell was transported by carrier gas (1 l min^{-1} He) and mixed with Ar (0.6 l min^{-1}) prior to entering the ICP. Helium (2 ml min^{-1}) was introduced to the collision cell of the mass spectrometer for minimization of spectral interferences. The tourmaline and allanite-(Ce) surface was ablated in individual spots for 50 and 20 seconds per spot, respectively, and by laser beam in diameter of 100 μm and 30 μm, respectively. Laser ablation was carried out using laser pulse fluence of 5 and 3.5 $J.cm^{-2}$ and 10 Hz repetition rate. The signals of isotopes of Li, Be, Mg, Sc, Mn, Y, Zr, Nb, Sn, REE, Hf, Ta, and Th for tourmaline and Li, Be, B, Sc, Y, Sn and La-Dy for allanite-(Ce) were measured. The contents of elements were calculated using NIST SRM 610 and 612 standards, and Si and Al as internal reference elements after baseline correction and integration of the peak area. The areas analyzed by LA-ICP-MS were carefully examined by the EMP prior to the laser ablation.

Raman spectroscopy

Raman spectra of REE-bearing epidote-group mineral were acquired on LabRAM HR Evolution (Horiba, Jobin Yvon) Raman spectrometer system. The Raman spectra were excited by 532 nm Nd:YAG and 633 nm He-Ne lasers and collected in range between 100 cm^{-1} and 1500 cm^{-1} with a resolution of 1 cm^{-1}. Repeated acquisitions were accumulated to improve spectral signal-to-noise ratio. Multiple spot analyses on different areas of REE-

bearing epidote-group mineral gave similar spectra and confirmed the spectral reproducibility. The laser spot for the 100x objective used provide approximately < 1 μm lateral and 2 μm horizontal resolution. No surface damage was observed after the laser illumination of the measurement. Due to lack of published Raman spectra of allanite, data for well crystalline allanite-(Nd) from Åskagen, Sweden (Škoda et al. 2012) were collected for a reference. The acquired Raman spectra were processed using Peakfit (Systat) software package. Band fitting was done using Pearson VII function with variable width; the fitting was gradually refined until it produced reproducible results with the square regression coefficient greater than 0.995.

RESULTS

Tourmaline textural and paragenetic types and their chemical composition

Prismatic crystals and grains of tourmaline, 1 mm to 3 cm in diameter, occur in the graphic unit, blocky K-feldspar, and in the albite unit. Based on the textural relations and chemical composition, three major tourmaline types were distinguished in the Kracovice pegmatite (Fig. 1); the types are slightly modified from those given by Čopjaková et al. (2013a). The list of tourmaline samples, their types, Y + REE contents, and their affiliations to the individual pegmatite zones are given in Table 1.

Primary (magmatic) Al-rich schorl (TurP1)

The volumetrically dominant black thick-prismatic tourmaline (TurP1) occurs in all pegmatite units except of the outermost granitic unit. The individual tourmaline grains typically are rather homogeneous in composition (Fig. 1). Dominant Al-rich schorl to very rare Al-rich fluor-schorl (6.57-7.12 apfu Al; 1.93-2.23 apfu Fe; 0.08-0.15 apfu Mn; $Fe_{tot}/(Fe_{tot} + Mg) \sim 0.98$; 0.24-0.68 apfu F) shows moderate to high X-site vacancy (0.27-0.46 pfu) and Na (0.52-0.70 apfu; Fig. 2, Table 2). Rare, homogeneous cores (TurP1c) darker in BSE with sharp contacts were observed particularly in schorl from the graphic unit (Fig. 1a). The cores (TurP1c) are slightly depleted in Na (0.49-0.58 apfu), Fe (1.88-2.08 apfu), Mn (0.07-0.10 apfu), Ca, Ti and F (0.18-0.37 apfu) compared to the TurP1 (Fig. 3; Table 2). Lithium contents determined by the LA-ICP-MS are low (80-500 ppm). The tourmaline shows slight deficit in ^{T}Si (~ 5.89 apfu Si in TurP1 and ~ 5.96 apfu Si in TurP1c) using normalization procedure based on 15 cations, which indicates minor incorporation of Al at the T-site. In general, the TurP1 tourmaline typically shows a limited compositional evolution on both the crystal (from core to rim) and the pegmatite (from the graphic unit to the albite unit) scales expressed as a slight enrichment in Na, Fe, Mn and F, and depletion in Mg (Fig. 3).

Primary (magmatic to hydrothermal) Li-rich fluor-schorl to fluor-elbaite (TurP2)

The tourmaline TurP2 forms overgrowths (up to 2 mm thick) around grains of the Al-rich schorl (TurP1); the TurP2 has sharp and straight contacts without any visible replacement textures (Fig. 1b,c). These overgrowths are typical for tourmaline from the blocky K-feldspar and albite units. Rarely, it forms small solitary prismatic crystals. Its chemical composition varies significantly, and corresponds to Li-rich fluor-schorl to fluor-elbaite, (LA-ICP-MS data yielded 0.1-1.1 wt. % Li). It has high Al (6.96-7.41 apfu) and Mn (0.18-0.76 apfu), highly variable Fe (0.25-1.82 apfu), and very low Mg (< 0.05 apfu). The X-site occupancy is dominated by Na (0.71-0.99 apfu) with very low Ca (≤ 0.03 apfu Ca; Fig. 2; Table 2). The amount of F at the W-site is high (0.67–1.00 apfu). Contents of Fe significantly decrease and Al, Mn, Na, F and Li increase toward rims of TurP2 crystals (Fig. 1b-d,3a, Table 2,3).

Secondary (hydrothermal) Li-rich fluor-schorl to fluor-elbaite (TurS)

Secondary tourmaline (TurS) typically replaces the primary Al-rich schorl (TurP1; Fig. 1) and rarely (in the albite unit) also the inner zones of the TurP2 adjacent to the TurP1 (Fig. 1c). The TurS is highly variable in texture. The replacement typically propagates from the crystal rim inwards (Fig. 1a) and along common microfractures (Fig. 1c,d). In contrast to the overgrowths of the primary Li-rich fluor-schorl to fluor-elbaite (TurP2), the replacement contacts are micro-lobulated, and the secondary tourmaline TurS locally contains numerous oval inclusions of quartz (Fig. 1a). The secondary tourmaline TurS occurs in all pegmatite units, but the most common and intensive replacement was observed in the graphic unit. However, the secondary tourmaline is compositionally almost identical to the texturally distinct primary Li-rich fluor-schorl to fluor-elbaite tourmaline TurP2 (Fig. 2,3, Table 2).

Concentrations of Sc and REE in tourmaline - LA-ICP-MS data

The individual types of tourmaline from the Kracovice pegmatite are generally characterized by variable and relatively high contents of Y+REE (3-458 ppm) and Sc (16-364 ppm; Fig. 4; Table 3). They show enrichment in LREE with nil to weak positive Ce anomalies (Ce/Ce* = 1.0-1.9) and deep negative Eu anomalies (Fig. 5a–c) in chondrite-normalized patterns. The highest Y+REE (40-458 ppm) and Sc (33-364 ppm) contents were found in the primary tourmaline TurP1 whereas the rare cores (TurP1c) contain significantly lower amounts of Y+REE (16-83 ppm) and Sc (50-194 ppm; Fig. 3,4,5a,b, Table 3). However, the La_N/Gd_N ratios in both types of the primary tourmaline TurP1c and TurP1 are similar (La_N/Gd_N 11-31

and 10-27, respectively). The contents of REE and Sc in the primary Al-rich schorl generally decrease and the Ce anomalies increase from the graphic unit towards the more evolved blocky K-feldspar and albite units (Table 3).

The primary Li-rich fluor-schorl to fluor-elbaite (TurP2) is significantly depleted in Y+REE (2.6-27 ppm) and has flatter Y+REE patterns (La_N/Gd_N = 2-15; Fig. 3,4,5, Table 3) compared to the TurP1. Chondrite-normalized REE patterns of TurP2 show negative Nd anomalies (0.54-0.91) indicating participation of tetrad effect; it is well visible in both the first (La-Nd) and the second (Sm-Gd) tetrads (Fig. 5c). Quantification of the tetrad effect using the parameters given by Irber (1999) or Monecke et al. (2002) was not possible due to the presence of Ce anomaly and too low concentrations of some HREE systematically below the detection limits. Scandium contents are also lower (21-56 ppm) compared to the TurP1 (Fig. 4, Table 3). The REE and Sc contents decrease and the tetrad effect seems to be more pronounced along the crystallization progress towards rims of TurP2 crystals (Fig. 3a).

In contrast to the TurP2, the secondary tourmaline (TurS) shows variable REE contents (5-384 ppm; Fig. 4, Table 3). Its chondrite-normalized patterns significantly vary; they range from those similar to the typical TurP2 to the more Y+HREE-enriched flatter patterns with lower La_N/Gd_N ratio (0.4-12; Fig. 5c). The Y+HREE-enriched patterns are typical for the secondary fluor-elbaite (TurS) replacing TurP1 (primary Al-rich schorl) altered to the secondary assemblage of REE-bearing epidote-group mineral + chamosite.

Replacement products of primary Al-rich schorl

Al-rich schorl (TurP1) is commonly partly replaced by the assemblage REE-bearing epidote-group mineral + chamosite. The replacement products are most common in the graphic unit and rather rare in more evolved units. The REE-bearing epidote-group mineral forms aggregates of prismatic crystals up 200 μm in size (Fig. 6). They occur exclusively in fractured tourmaline TurP1 which is partly replaced by a F,Na-rich variety of the secondary fluor-elbaite (Fig. 3b,6). The assemblage of REE-bearing epidote-group mineral + chamosite was not observed in those grains of the primary Al-rich schorl which (i) were not altered, or (ii) were partly replaced by the secondary tourmaline (TurS) characterized by lower contents of Na, F and Li (Fig. 3b). The replacement assemblage is absent exterior of the tourmaline (TurP1); instead, minute crystals (≤ 5 μm) of hydrated arsenate of Y+HREE locally occur around the tourmaline replaced by the REE-bearing epidote-group mineral.

REE-bearing epidote-group mineral

The mineral has Y+REE ranging from 0.42 to 0.60 apfu, with the most frequent value of ~ 0.57 apfu (Table 4). Majority of 43 EMP analytical points belongs to the allanite subgroup (with Y+REE > 0.5 apfu), only five of them correspond to the clinozoisite subgroup (with Y+REE < 0.5 apfu). In all EMP analyses, Ce (0.19-0.35 apfu) predominates over other REE and Y; the EMP analyses are in a good agreement with the results of LA-ICP-MS. The mineral has steep LREE-rich chondrite-normalized REE patterns (avg. La_N/Gd_N ~ 43) with significantly negative Eu anomalies (Eu contents < 1 ppm; Fig. 5d). The contents of La negatively correlate with Nd (and MREE) and therefore the chondrite-normalized REE patterns vary between steep La-rich domains usually present in central parts of the aggregates and Nd- and MREE-rich ones (Fig. 5d,7) found in the aggregate rims. Elevated contents of Mn (0.62-1.55 wt. % MnO) and Sr (0.22-1.15 wt. % SrO) are typical. The M-sites are dominated by Al (2.05–2.50 apfu) and Fe (0.44-0.64 apfu), and contain extraordinarily high contents of Sc (≤ 3.26 wt. % Sc_2O_3; ≤ 0.25 apfu) and Sn (≤ 1.05 wt. % SnO_2). Other analyzed elements (Th, U, Na, K, P, Mg, Pb, Ba, Cr, V, HREE, and Cl) are very close or below the detection limits of EMP except for Ti (≤ 0.43 wt. % TiO_2) and F (≤ 0.23 wt. %). A significant and variable vacancy occurs in the M-sites (□cations = 2.76-2.99 apfu; Table 4). A detailed WDX angle scan excluded presence of other elements detectable by EMP that could possibly enter the structure of allanite (Ga, Ge, Zn) in a significant amount. The contents of light elements detected by LA-ICP-MS are rather low (B < 320 ppm; Be 50-175 ppm; Li < 11 ppm). The highest contents of Sc are typical for the central parts of aggregates, whereas the outer parts are Sc-poor (Fig. 7). In general, the contents of Sc and La decrease and MREE and Y increase from the graphic towards the blocky K-feldspar and albite units (Table 4).

Raman spectroscopy

The Raman spectrum of the REE-bearing epidote-group mineral from Kracovice shows several distinct bands. The strongest vibrations occur at 1064, 1048, 971, 927, 875, 687, 569, 458, 427 and 358 cm^{-1} and the spectrum matches well the spectrum of the crystalline allanite-(Nd) from Åskagen (Fig. 8). The fairly narrow vibration bands indicate its good crystallinity. The vibration bands in the regions 1100-830, ~ 570 and 500-300 cm^{-1} are identical with the spectra of epidote published by Makreski et al. (2007) and Wang et al. (1994). Makreski et al. (2007) interpreted the highest-frequency bands in the region 1100-800 cm^{-1} as a symmetric stretching Si-O_{nb} (O_{nb}-non bridging oxygen) from the $(Si_2O_7)^{-6}$ and $(SiO_4)^{-4}$ groups. According to Wang et al. (1994), the symmetric stretching Si-O_b-Si bonds (O_b-bridging

337 oxygen) should be expected in the 750-450 cm^{-1} region. Bands in the 550-300 cm^{-1} region
338 should correspond to the vibrations of M-O bonds according to Makreski et al. (2007).
339
340 Chamosite
341 The chamosite has rather uniform ^{T}Si (2.71-2.85 apfu) and ^{M}Al (1.45-1.56 apfu), and variable,
342 negatively correlated Fe and Mn contents (Fe = 3.18-3.76 apfu, Mn = 0.23-0.75 apfu)
343 indicating homovalent substitution $FeMn_{-1}$. Magnesium is present in rather low amounts (Mg
344 ~ 0.37 apfu) and the contents of Sc, F, and Cl are below the detection limit of EMP.
345
346 ## DISCUSSION
347 ### Compositional evolution of tourmaline, and Y+REE and Sc variations
348 Concentrations and distributions of Y+REE in tourmaline are controlled mainly by: (i) total
349 contents of REE in granitic melt, (ii) crystallization sequence of REE-bearing accessory
350 minerals (Torres-Ruiz et al. 2003; Raith et al. 2004; Čopjaková et al. 2013a), and/or (iii)
351 composition of hydrothermal fluids (King et al. 1988; Jiang et al. 2004; Garda et al. 2010;
352 Čopjaková et al. 2013b). The contents of Y+REE in tourmaline from granitic pegmatites are
353 generally low (< 30 ppm, Jolliff et al. 1987; Hellingwerf et al. 1994; Roda et al. 1995; Kontak
354 et al. 2002); hence, the concentrations of Y+REE in tourmaline from the Kracovice pegmatite
355 (up to 458 ppm) are among the highest reported to date. Only the unusual REE-enriched
356 dravite from the granitic pegmatite at Forshammar (Sweden) attains higher contents (ΣREE =
357 100-1200 ppm; Bačík et al. 2012).
358
359 Primary (magmatic) Al-rich schorl (TurP1, TurP1c)
360 Chemical composition and textural relations of the Al-rich schorl suggest that it crystallized
361 early from melt (Novák et al. 2012; Čopjaková et al. 2013a). The presence of magmatic
362 tourmaline and hambergite indicates high activity of B in the melt (Wolf and London 1997).
363 Crystallization of the magmatic tourmaline was terminated either by melt depletion in Fe, or
364 due to decrease of B content in the melt as a result of precipitation of B-rich minerals and/or
365 by partitioning of B into exsolved vapor.
366 Similarities between the REE patterns in magmatic tourmaline and the whole-rock
367 composition were documented from granites, pegmatites and orthogneisses worldwide (e.g.
368 Torres-Ruiz et al. 2003; Raith et al. 2004; Pesquera et al. 2005; Čopjaková et al. 2013a).
369 Partition coefficients for REE between tourmaline and silicate melt are invariably close to 1
370 suggesting that magmatic tourmaline does not selectively incorporate any specific REE into

its crystal structure (van Hinsberg 2011; Čopjaková et al. 2013a). Increased content of REE+Sc in the magmatic tourmaline TurP1 compared to the early magmatic cores of TurP1c can reflect an enrichment of REE+Sc in the melt during a progressive crystallization of major rock-forming minerals without early precipitation of Y+REE-rich accessory minerals. A similar trend was observed in tourmaline from NYF pegmatites of the Třebíč Pluton (Čopjaková et al. 2013a). The magmatic tourmaline TurP1 shows a decrease in REE contents from the graphic to the blocky K-feldspar and albite units (Fig. 4a,5a-b, Table 3) reflecting progressive crystallization of the pegmatite melt and fractional crystallization of REE-enriched accessory minerals. This is consistent with the trend reported by Jolliff et al. (1987).

The concentrations of Sc (up to 364 ppm) in the magmatic tourmaline (TurP1) from the Kracovice pegmatite are among the highest published to date. The only higher Sc contents were reported in V-rich oxy-dravite from graphitic quartzites at Bítovánky, and from NYF euxenite-type pegmatites of the Třebíč Pluton (≤ 1290 ppm and 765 ppm respectively; Cempírek et al. 2013; Čopjaková et al. 2013a), which are both located nearby the studied locality within the Třebíč region. The evolutionary trends of Sc in tourmaline correlate well with the REE contents (Fig. 4) reflecting their similar geochemical behavior. Tourmaline seems to be an effective sink of Sc from melt under specific circumstances (see Čopjaková et al. 2013a). This does not match with the relatively low experimentally determined distribution coefficients for Sc ($D_{tu/melt}$ ~ 0.71, van Hinsberg 2011); however, the contrasting Sc behavior in pegmatitic tourmaline can be explained by the difference in melt composition and in the degree of melt undercooling compared to the experimental conditions.

Li-rich fluor-schorl to fluor-elbaite (TurP2 and TurS)

The distinct compositional gap between the magmatic Al-rich schorl (TurP1) and the Li-rich tourmaline (both TurP2 and TurS) indicates a time gap between their crystallization and a significant difference in conditions of their crystallization. The abrupt change from Fe,REE-rich and Na,F,Li-poor magmatic Al-rich schorl to Fe,REE-poor, Li,F,Na-rich fluor-schorl to fluor-elbaite is well documented on Fig. 3. London (2014a,b) explains the abrupt transition in pegmatite melt composition by final consummation of the undercooled Fe-bearing bulk melt in the pegmatite core by the boundary layer liquid, and its depletion in Fe by the end of primary crystallization. It is followed by crystallization of the boundary layer liquid in the pegmatite core which has sodic, alkaline composition, and it is enriched in fluxing components (B, P, and F), water (H), and rare alkalis (Li, Rb, Cs). Both textural types of Li-rich tourmaline (overgrowing - TurP2 and replacing - TurS) are characterized by very similar

chemical composition and compositional trends (Fig. 3) reflecting their rather coeval formation.

The textural relations of the primary Al-rich-schorl (TurP1) and the overgrowing primary Li-rich tourmaline (TurP2) from the blocky K-feldspar and the albite unit (Fig. 1b-d) suggest crystallization of the TurP2 from a highly evolved, F,Li-rich source. Textural evidence indicates that its crystallization proceeded before complete solidification of the host environment, and the sequence of its crystallization may represent the transition from the late magmatic to early hydrothermal conditions, i.e. early crystallization from the fractionated melt (boundary layer liquid; London 2014a,b) in the pegmatite core. Gradual changes of chemical composition of TurP2 reflect evolution of the host environment during its prolonged crystallization. Textural relations and tourmaline composition (Fig. 1c,d,3) indicate coeval crystallization of the outermost part of TurP2 (the darkest rim on Fig.1) and the replacing F,Li-rich tourmaline TurS from the same hydrothermal fluid.

The secondary Li-rich tourmaline (TurS) showing irregular contacts and replacement features (Fig. 1a) is most likely of hydrothermal origin and is interpreted as the product of a subsolidus reaction of fractured Al-rich schorl (TurP1) and rarely TurP2 with evolved pegmatite-derived fluids migrating along grain boundaries and fractures from the central part of the dike. Local differences and evolution in chemical composition of TurS (see Fig. 3) reflect gradually inhomogeneous composition of the reacting hydrothermal fluid (increasing Li, F, Na, decreasing Fe) and the composition of reacting tourmaline. The reason for fracturing of the early solidified units is not clear; it could be triggered by vapor exsolution from the residual melt in the pegmatite core, and loss of aqueous fluid to the host rock (cf. London 2013). Textural differences (overgrowing TurP2 *versus* replacing TurS) reflect either the degree of solidification of the melt or differences in local activity of B in fluids.

Generally, low REE contents are expected in tourmaline crystallized from late melt-derived hydrothermal fluids relative to the associated melt-derived tourmalines (Jolliff et al. 1987; Pesquera et al. 2005). It is consistent with the REE evolution in Li-rich tourmaline (TurS and probably TurP2 as well) showing commonly very low Y+HREE contents. Anomalous, significantly HREE,Y-enriched patterns (flatter than those of TurP2; Fig. 5c) were locally observed in the secondary tourmaline (TurS); they reflect local enrichment of these elements in fluids. The HREE+Y were probably released during replacement of the primary tourmaline (TurP1); no other significant local Y+HREE source was observed. Rarely, similar HREE-enrichment was observed in the secondary tourmaline (TurS) replacing garnet (Čopjaková et al. 2014), but only very close to the replaced garnet. This indicates a very

limited Y+HREE mobility in the pegmatite-derived fluids where the Y+HREE enter directly to the fluor-elbaite (TurS) structure and yield a tourmaline with flat HREE+Y-enriched patterns. Alternatively, the anomalous patterns could be caused by submicroscopic (below the resolution of EMP) inclusions of a Y+HREE-bearing mineral (hydrated Y+HREE arsenate) enclosed in the fluor-elbaite; small inclusions of hydrated Y+HREE arsenates were sporadically observed around partially replaced magmatic tourmaline or garnet but never in relation to the overgrowing Li-rich tourmaline (TurP2). Intensive replacement of the REE-rich tourmaline (TurP1) could produce a small volume of REE-bearing epidote-group mineral along with a rare submicroscopic Y+HREE phase because the source tourmaline has lower LREE/HREE ratio compared to the secondary REE-bearing epidote-group mineral.

Tetrad effect in tourmaline

The REE patterns of the Li-rich tourmaline (both types TurP2 and TurS; Fig. 5c) as well as the patterns of other REE-bearing minerals in the Kracovice pegmatite (unpublished data of authors) which crystallized either from viscous melt (garnet I, zircon), or from flux-rich liquid (TurP2, garnet II), or from melt-derived hydrothermal fluids (TurS), exhibit M-type tetrad effect. Tetrad effect is typical for highly evolved volatiles-rich (e.g., F, H_2O) melts at the final stages of crystallization when F-rich aqueous fluid phase is exsolved from the melt (Irber 1999; Dolejš and Štemprok 2001) or when an F-bearing hydrosaline magmatic liquids are separated from granitic magma above its solidus (Veksler et al. 2005; Peretyazhko and Savina 2010; Wu et al. 2011; Cao et al. 2013). A possible factor contributing to the tetrad effect is a fluorine complexation (Irber 1999). M-type tetrads are common in the minerals crystallized from residual silicate melt. In contrast, the exsolved F-rich hydrosaline liquids (according to Veksler et al. 2005; Peretyazhko and Savina 2010; Wu et al. 2011; Cao et al. 2013) or F-rich aqueous fluid (according to Irber 1999; Dolejš and Štemprok 2001) could extract REE and acquire a W-type tetrad effect complementary to the pattern in the silicate melt.

Evolution of REE patterns in tourmaline (from TurP1, through TurP2 and TurS) indicate clearly that tetrad effect is not an original feature of the pegmatitic magma; instead, it gradually evolves during melt crystallization and related processes. Exsolution of fluoride melt with high contents of REE and W-type tetrad effect is one of likely mechanisms yielding the residual melt with M-type tetrad effect. Topaz, a common accessory to minor mineral in the more fractionated units of the Kracovice pegmatite, could hypothetically crystallize from such a fluoride melt. However, topaz is REE-poor (~ 23 ppm) with a flat REE pattern (La_N/Yb_N ~ 2.0-3.1) and it is not associated with any REE-bearing mineral; therefore, the

topaz data did not provide any convincing evidence for its crystallization from a REE-rich fluoride melt with W-type tetrad effect.

There is no direct mineralogical evidence that exsolution of F-rich aqueous fluids with complementary W-type tetrad effect (according to Irber 1999; Dolejš and Štemprok 2001) from flux-rich melt is responsible for the development of the M-type tetrad effect in the studied pegmatite body. The secondary tourmaline (TurS) which crystallized from F-rich hydrothermal fluids shows the M-type REE tetrad effect. If it crystallized from such aqueous fluids, then it did not retain their ideal W-type REE pattern and acquired the opposite M-type REE pattern instead. M-type REE tetrad effect in fluorite precipitated from melt-derived hydrothermal fluids was earlier reported by Monecke et al. (2002) and Badanina et al. (2006).

The replacement process of the primary tourmaline

Tourmaline is considered to be a refractory mineral (Henry and Dutrow 1996; London 2011). However, black schorlitic tourmaline in granitic pegmatites is rarely replaced by secondary phases: e.g., muscovite (Dietrich 1985; Ahn and Buseck 1998; Novák et al. 2011b); pumpellyite-(Al) + chlorite, K-feldspar (Prokop et al. 2013) or chlorite + titanite (Novák et al. 2013). In contrast, metasomatic replacement of elbaite by lepidolite or borocookeite is more common (e.g. Beurlen et al. 2011; Novák et al. 2011b). Tourmaline breakdown commonly reflects the input of alkaline, high-pH and B-undersaturated fluids (Morgan and London 1989; Ahn and Buseck 1998; London 2011; Čopjaková et al. 2012).

Mineral textures and chemical composition of tourmaline indicate replacement of the Al-rich schorl (TurP1) during its interaction with highly evolved Li,F-rich, alkaline (high Na) and B-saturated pegmatite-derived fluids. These fluids most likely originated by exsolution from the residual flux-rich silicate melt in the pegmatite center; the process probably caused intensive hydrofracturing (brecciation) of early-crystallized units with Al-rich schorl (TurP1) and formation of the secondary assemblage according to the simplified scheme:

REE-rich Al-rich schorl + Li,F-rich aqueous fluids → fluor-elbaite + REE-bearing epidote-group mineral + chamosite.

The paragenetic link between the amount of the REE-bearing epidote-group mineral and concentrations of REE in the magmatic tourmaline TurP1 as well as their spatial relations indicate that REE and Sc necessary for the formation of the Sc-rich REE-bearing epidote-group mineral were released during dissolution of the Al-rich schorl (TurP1). Generally low contents of REE and Sc in Li-rich tourmaline (TurP2 and TurS) suggest depletion of melt-derived hydrothermal fluids in REE and Sc; any external input of Y+REE and Sc is unlikely.

Taking into account the average composition of the Al-rich schorl (TurP1) and the REE-bearing epidote-group mineral, and assuming no external input of REE, we calculated the mass-balance between the parental Al-rich schorl and the daughter REE-bearing epidote-group mineral. For precipitation of 1 mol of REE-bearing epidote-group mineral, it is necessary to alter ~ 460 mols of TurP1. Taking into account different densities of allanite and schorl (3.7 and 3.2 g.cm-3, respectively; Anthony et al. 2011) the mass balance calculation shows that alteration of a 900 μm-side cube of the TurP1 releases enough REE and Sc to form a 100 μm-side cube of the REE-bearing epidote-group mineral, which roughly corresponds to the textural relations observed in BSE (Fig. 6).

Crystal chemistry of REE-bearing epidote-group mineral

Natural REE-bearing members of the epidote group of minerals are quite commonly metamict due to their elevated contents of Th and U; the radiation damage is typically accompanied by hydration and loss of cations (Gieré and Sorensen 2004; Čobić et al. 2010). The high oxide totals observed in the Sc-rich REE-bearing epidote-group mineral (Table 4) contraindicate significant hydration and its non-metamict nature was also confirmed by the Raman spectroscopy (Fig. 8).

A-sites occupancy

The LREE-enriched patterns of the REE-bearing epidote-group mineral are steeper compared to those of the REE-rich magmatic tourmaline; the increased pattern slope manifests strong fractionation of LREE from HREE in allanite (Brooks et al. 1981; Chesner and Ettlinger 1989). Moreover, pronounced negative Eu anomaly is typical for allanite (Gieré and Sorensen 2004). Manganese can occur in both divalent and trivalent states and it can enter three different sites (A1, M1, M3; Bonazzi et al. 1996; Gieré and Sorensen 2004). In our samples, Mn negatively correlates with Ca and most likely enters the A site. Small surplus of cations in the A sites when all Mn is assigned to the A1 site (avg. ∑cations in that case = 2.02 apfu) indicates that part of Mn (Mn^{2+}or Mn^{3+}) could be present in the M-sites.

M-sites occupancy

Scandium in epidote-group minerals has been reported in dissakisite from the pegmatite at Impilaks, Finland (wet analysis, ~ 1 wt. % Sc_2O_3; Meyer 1911) and in allanite-(Ce) from the Crystal Mountains, Montana, USA (EMP analysis, 0.5 wt. % Sc_2O_3; Foord et al. 1993). Scandium content in the REE-bearing epidote-group mineral from the Kracovice pegmatite (≤

3.26 wt. % Sc_2O_3; ≤ 0.25 apfu) is the highest reported to date. The negative correlation Al/Sc (slope of the regression line ~ 1) suggests that Sc enters the octahedral site by the substitution $ScAl_{-1}$; this is also supported by the fully occupied A-sites with Ca, REE, Sr and Mn. High Sc contents are typical for domains rich in La, and Sc negatively correlates with Nd (Fig. 9a,b).

Tin is fairly common trace element in allanite (< 0.85 wt. % SnO_2; Gieré and Sorensen 2004); the REE-bearing epidote-group mineral from the Kracovice pegmatite shows the highest Sn contents (up 1.05 wt. % SnO_2) found in allanite. The mechanism of Sn incorporation in the M-sites by the substitution $Sn^{4+}Fe^{2+}$ $(Fe^{3+},Al^{3+})_{-2}$ has been described for epidote by van Marcke de Lummen (1986) but the chemical complexity of the studied REE-bearing epidote-group mineral does not allow to elucidate the exact Sn substitution scheme.

Allanite can incorporate trace to minor contents of Be (up 2.5 wt. % BeO; Iimori 1939; Quensel 1945; Kimura and Nagashima 1951); however, the presence of Be in detectable amounts has not been confirmed by *in situ* analytical techniques (Hermann 2002). The LA-ICP-MS data of Sc-rich REE-bearing epidote-group mineral from Kracovice yielded low contents of Be (50-175 ppm) but it is not clear whether Be substitutes for Al in the M-sites or enters the T-site (Iimori 1939; Shannon 1976).

The sum of cations in the M-sites of the REE-bearing epidote-group mineral from the Kracovice pegmatite is often lower than 3 apfu (2.79-3.03 apfu, Table 4); on the other hand, careful control analyses of other minerals of the epidote group (epidote, Vlastějovice, Czech Republic; allanite-(Nd), Åskagen, Sweden; ferriallanite-(Ce), Nya Bastnäs, Sweden) yielded the average sum 3.007 apfu. Detailed WDX angle scan excluded presence of other unanalyzed elements detectable by EMP in significant amount. Moreover, the contents of Li, Be and B (Li ≤ 11 ppm, Be 50-175 ppm, B ≤ 320 ppm) obtained by LA-ICP-MS cannot significantly affect the sum of cations in the M-sites. Therefore, our observations strongly indicate a vacancy in the M-sites. The M-site vacancy correlates positively with (Y+REE)-Fe^{2+} (Fig. 9c) which represents the surplus of incorporated REE beyond the allanite substitution $REE^{3+}Fe^{2+}Ca^{2+}_{-1}R^{3+}_{-1}$ where R^{3+} = Al, Fe^{3+}. Moreover, Y+REE does not significantly change with variable R^{3+} in the M-sites (Fig. 9d), whereas (Y+REE)-Fe^{2+} and vacancy in the M-sites show a good negative correlation with Al^{3+} (Fig. 9e,f). The observed correlations indicate two types of REE substitutions in the structure of the REE-bearing epidote-group mineral: the allanite substitution (1) $REE^{3+}Fe^{2+}Ca^{2+}_{-1}R^{3+}_{-1}$ (where R^{3+} = Al, Fe^{3+}) and the substitution (2) $^{A}REE^{3+}{}_{3}{}^{M}\square_{1}{}^{A}Ca_{-3}{}^{M}Al^{3+}_{-1}$ involving vacancy in the M-sites. The electron microprobe data and the observed substitutions trends seem to indicate existence of the theoretical end-member $CaREEAl_2R^{3+}_{2/3}\square_{1/3}[Si_2O_7][SiO_4](O)(OH)$ of the allanite subgroup. It is clear (Fig. 10) that

575 the content of the clinozoisite subgroup end-members is rather constant and the studied REE-
576 bearing epidote-group mineral generally follows the substitution trend $R^{3+}_2\square_1R^{2+}_{-3}$ from
577 allanite-(Ce) to the $CaREEAl_2R^{3+}_{2/3}\square_{1/3}[Si_2O_7][SiO_4](O)(OH)$ end-member. However, an
578 exact determination of the Fe^{2+}/Fe^{3+} ratio is necessary to support the conclusions.
579
580 **IMPLICATIONS OF THE STUDY**
581 This study has been focused on the major- to trace-element compositional changes in
582 tourmaline growth history from magmatic to hydrothermal crystallization stage and
583 tourmaline alteration processes. Compositional trends in tourmaline based on EMP data are
584 widely used as indicators of geological processes (e.g., Henry and Dutrow 1996; van
585 Hinsberg et al. 2011). The results of this work confirm high sensitivity of Y+REE contents in
586 tourmaline to the composition of its host rocks, source melt, and hydrothermal fluids.
587 Consequently the Y+REE contents in tourmaline seem to be an ideal tool for petrogenetic
588 interpretations as well as for provenance studies of sedimentary rocks. Tourmaline can also
589 serve as an effective sink for Sc from granitic melt and represents another important carrier of
590 Sc along with other Fe-Mg minerals (e.g. amphibole- or pyroxene-group minerals).
591 This study also revealed the continuous evolution of the M-type tetrad effect from the
592 REE-patterns without tetrad effect to the well evolved M-type tetrad effect in the course of
593 tourmaline crystallization. This clearly indicates the tetrad effect gradually evolves during the
594 progressive solidification of the melt and related processes and the M-type pattern gradates to
595 the metasomatic/hydrothermal stage. The mechanism of formation of the tetrad effect remains
596 still unclear (Irber 1999; Veksler et al. 2005), but it is obviously connected to fluorine
597 complexation in highly evolved volatiles-rich (e.g., F, H_2O) melts.
598 The primary magmatic REE-enriched tourmaline (schorl) was partially replaced by the
599 assemblage of REE-bearing epidote-group mineral + chamosite + fluor-elbaite during its
600 interaction with Li,F-rich fluids. Schorlitic tourmaline generally shows a large stability field
601 and is usually considered to be resistant to hydrothermal alteration and weathering; this study
602 shows that low-temperature hydrothermal alteration and replacement reactions of tourmaline
603 and factors affecting its instability during elevated activity of hydrothermal fluid in early
604 subsolidus stage remain an important direction for future research.
605 The formation of the REE-rich secondary minerals is commonly coupled to alteration
606 of primary REE-rich minerals (e.g. monazite, xenotime, allanite, titanite, garnet, zircon).
607 However, the source of desirable REE for the formation of REE-minerals could be a

608 nominally REE-free mineral; in this study the source of REE+Sc for Sc- and REE-bearing
609 epidote-group mineral seems to be tourmaline.
610 The unusual chemical composition of REE-bearing epidote-group mineral replacing
611 magmatic schorl (enrichment in Sc and Sn) indicates that those elements should be sought
612 during developing of the analytical setup routines for measuring of epidote-group minerals.
613 The Sc content can be easily overlooked in the energy-dispersive spectrum because the Sc *K*α
614 peak coincides with the Ca *K*β line. Possibility of vacancy in the M-sites should be taken into
615 account. Inconsistent stoichiometry of allanite-subgroup minerals can be in some cases caused
616 by vacancy in the M-sites, instead of the more usual explanations such as alteration of
617 metamict allanite or presence of some non-analyzed elements.
618
619 **ACKNOWLEDGEMENTS**

620 The authors are very grateful to Adam Pieczka and to the unknown reviewer for constructive
621 criticism that improved the manuscript. The authors thank Fernando Colombo for editorial
622 handling. This paper was supported by the research project GAČR P210/10/0743 to RČ, RŠ
623 and MN. MVG acknowledges the European Regional Development Fund project "CEITEC"
624 (CZ.1.05/1.1.00/02.0068). JC acknowledges support of the Ministry of Culture of the Czech
625 Republic (as part of its long-term conceptual development program for research institutions,
626 the Moravian Museum, MK000094862).
627
628 **REFERENCES**

629 Ahn, J.H., and Buseck, P.R. (1998) Transmission electron microscopy of muscovite alteration
630 of tourmaline. American Mineralogist, 83, 535-541.
631 Anthony, J. W., Bideaux, R. A., Bladh, K. W., & Nichols, M. C. (2011). Handbook of
632 Mineralogy, Mineralogical Society of America, Chantilly, USA.
633 Armbruster, T., Bonazzi, P., Akasaka, M., Bermanec, V., Chopin, Ch., Gieré, R., Heuss-
634 Assbichler, S., Liebscher, A., Menchetti, S., Pan, Y., and Pasero, M. (2006)
635 Recommended nomenclature of epidote-group minerals. European Journal of
636 Mineralogy, 18, 551-567.
637 Bačík, P., Uher, P., Ertl, A., Jonsson, E., Nysten, P., Kanický, V., and Vaculovič, T. (2012)
638 Zoned REE-enriched dravite from a granitic pegmatite in Forshammar, Bergslagen
639 Province, Sweden: an EMPA, XRD and LA–ICP–MS study. Canadian Mineralogist,
640 50, 825-841.

641 Badanina, E.V., Trumbull, R.B., Dulski, P., Wiedenbeck, M., Veksler, I.V., and Syritso, L.M.
642 (2006) The behavior of rare-earth and lithophile trace elements in rara-metal granites:
643 A study of fluorite, melt inclusions and host rocks from the Khangilay complex,
644 Transbaikalia, Russia.. Canadian Mineralogist, 44, 667-692.
645 Beurlen, H., De Moura, O.J.M., Soares, D.R., Da Silva, M.R.R., and Rhede, D. (2011)
646 Geochemical and Geological controls on the genesis of gem-quality "Paraiba
647 tourmaline" in granitic pegmatites from Northeastern Brazil. American Mineralogist,
648 49, 277-300.
649 Bonazzi, P., Menchetti, S., and Reinecke, T. (1996) Solid solution between piemontite and
650 androsite-(La), a new mineral of the epidote group from Andros Island, Greece.
651 American Mineralogist, 81, 735-742.
652 Brooks, C.K., Henderson, P., and Rønsbo, J.G. (1981) Rare-earth partition between allanite
653 and glass in the obsidian of Sandy Braes, Northern Ireland. Mineralogical Magazine,
654 44, 157-160.
655 Cao, M.-J., Zhou, Q.-F., Qin, K.-Z., Tang, D.-M., and Evans, N.J. (2013) The tetrad effect
656 and geochemistry of apatite from the Altay Koktokay No. 3 pegmatite, Xinjiang,
657 China: implications for pegmatite petrogenesis. Mineralogy and Petrology, 107, 985-
658 1005.
659 Cempírek J, Houzar S, Novák M, Groat LA, Selway JB, and Šrein V (2013) Crystal structure
660 and compositional evolution of vanadium-rich oxy-dravite from graphite quartzite at
661 Bítovánky, Czech Republic. Journal of Geosciences, 58, 149-162.
662 Černý, P., and Ercit, T.S. (2005) Classification of granitic pegmatites. Canadian Mineralogist,
663 43, 2005-2026.
664 Černý, P., London, D., and Novák, M. (2012) Granitic pegmatites as reflections of their
665 sources. Elements, 8, 289-294.
666 Chesner, C.A., and Ettlinger, A.D. (1989) Composition of volcanic allanite from the Toba
667 Tuffs, Sumatra, Indonesia. American Mineralogist, 74, 750-758.
668 Čobić, A., Bermanec, V., Tomašić, N, and Škoda, R. (2010) The hydrothermal
669 recrystallization of metamict allanite-(Ce). Canadian Mineralogist, 48, 513-521.
670 Čopjaková, R., Škoda, R., and Buriánek, D. (2012) Hydrothermal alteration of tourmaline
671 from tourmalinites in the Krkonoše Crystalline Unit, Bohemian Massiff, Czech
672 Republic. Acta Mineralogica-Petrographica, Abstract Series, Szeged, 7, 30.
673 Čopjaková, R., Škoda, R., Vašinová Galiová, M., and Novák, M. (2013a) Distributions of Y +
674 REE and Sc in tourmaline and their implications for the melt evolution; examples

675 from NYF pegmatites of the Třebíč Pluton, Moldanubian Zone, Czech Republic.
676 Journal of Geosciences, 58, 113-131.
677 Čopjaková, R., Škoda, R., Novák, M., and Vašinová Galiová, M. (2013b) Geochemistry of Y
678 + REE in stratiform tourmalinites and their tourmalines: implications for their genesis.
679 In: Jonsson E. (ed) Mineral deposit research for a high-tech world, Vols. 1-4, 12th
680 Biennial SGA Meeting on Mineral Deposit Research for a High-Tech World Uppsala,
681 SE, Uppsala University,1705-1708.
682 Čopjaková, R., Škoda, R., Vašinová Galiová, M., and Novák, M. (2014) Behaviour of B and
683 Li during the evolution of the Kracovice pegmatite related to the formation and
684 stability of tourmaline and garnet. CEMC 2014 Book of abstracts, 21-22.
685 Coulson, I.M. (1997) Post-magmatic alteration in eudialyte from the North Qoroq center,
686 South Greenland. Mineralogical Magazine, 61, 99-109.
687 Dietrich, R.V. (1985) The Tourmaline Group. Van Nostrand Reinhold, New York, p 300.
688 Dolejš, D., and Štemprok, M. (2001) Magmatic and hydrothermal evolution of Li-F granites:
689 Cínovec and Krásno intrusions, Krušné hory batholith, Czech Republic. Bulletin of the
690 Czech Geological Survey, 76, 77-99.
691 Foord, E.E., Birmingham, S.D., Demartin, F., Pilati, T., Gramaccioli, C.M., and Lichte, F.E.
692 (1993) Thortveitite and associated Sc-bearing minerals from Ravalli County, Montana.
693 Canadian Mineralogist, 31, 337-346.
694 Garda, G.M., Beljavskis, P., D'Agostino, L.Z., and Wiedenbeck, M. (2010) Tourmaline and
695 rutile as indicators of a magmatic-hydrothermal origin for tourmalinite layers in the
696 São José do Barreiro Area, NE Ribeira Belt, Southern Brazil. Geol USP Sér cient São
697 Paulo, 10, 97-117.
698 Gieré, R., and Sorensen, S.S. (2004) Allanite and other REE-rich epidote-group minerals.
699 Reviews in Mineralogy and Geochemistry, 10, 56, 431-493.
700 Hawthorne, F.C., and Henry, D.J. (1999) Classification of the minerals of the tourmaline
701 group. European Journal of Mineralogy, 11, 201-215.
702 Hellingwerf, R.H., Gatedal, K., Gallagher, V., and Baker, J.H. (1994) Tourmaline in the
703 central Swedish ore district. Mineralium Deposita, 29, 189-205.
704 Henry, D.J., and Dutrow, B.L. (1996) Metamorphic tourmaline and its petrologic
705 applications. In: Grew E.S. and Anovitz L.M. (eds) Boron: Mineralogy, Petrology and
706 Geochemistry. Mineralogical Society of America Reviews on Mineralogy, 33, 503-
707 557.

Henry, D.J., Novák, M., Hawthorne, F.C., Ertl, A., Dutrow, B.L., Uher, P., and Pezzotta, F. (2011) Nomenclature of the tourmaline-group minerals. American Mineralogist, 96, 895-913.

Hermann, J. (2002) Allanite: thorium and light rare earth element carrier in subducted crust. Chem Geol 192: 289-306.

Hoshino, M., Kimata, M., and Shimizu, M. (2006) Allanite-(Ce) in granitic rocks from Japan: genetic implications of patterns of REE and Mn enrichment. Canadian Mineralogist, 44, 45-62.

Iimori, T. (1939) A Beryllium-bearing variety of allanite. Scientific Papers of the Institute of physical and chemical Research, Tokyo, 36, 53-55.

Irber, W. (1999) The lanthanide tetrad effect and its correlation with K/Rb, Eu/Eu*, Sr/Eu, Y/Ho, and Zr/Hf of evolving peraluminous granite suites. Geochimica et Cosmochimica Acta, 63, 489-508.

Janoušek, V., and Holub, F.V. (2007) The causal link between HP-HT metamorphism and ultrapotassic magmatism in collisional orogens: case study from the Moldanubian Zone of the Bohemian Massif. Proceedings of the Geologists Association, 118, 75-86.

Jiang, S.-Y., Yu, J.-M., and Lu, J.-J. (2004) Trace and rare-earth element geochemistry in tourmaline and cassiterite from the Yunlong tin deposit, Yunnan, China: implication for migmatitic–hydrothermal fluid evolution and ore genesis. Chemical Geology, 209, 193- 213.

Jolliff, B.L., Papike, J.J., and Laul, J.C. (1987) Mineral recorders of pegmatite internal evolution: REE contents of tourmaline from the Bob Ingersoll pegmatite, South Dakota. Geochimica et Cosmochimica Acta, 51, 2225-2232.

Kimura, K., and Nagashima, K. (1951) Chemical investigations of Japanese minerals containing rarer elements. XLII Journal of the Chemical Society of Japan, Pure Chemistry Sections, 72, 52-54 (in Japanese).

King, R.W., Kerrich, R.W., and Daddar, R. (1988) REE distributions in tourmaline: an INAA technique involving pretreatment by B volatilization. American Mineralogist, 73, 424-431.

Kontak, D.J., Dostal, J., Kyser, K., and Archibald, D.A. (2002) A petrological, geochemical, isotopic and fluid inclusion study of 370 Ma pegmatite–aplite sheets, Peggys Cove, Nova Scotia, Canada. Canadian Mineralogist, 40, 1249-1286.

Leitch, C.H.B., and Turner, R.J.W. (1992) Preliminary field and petrographic studies of the sulphide-bearing network underlying the western orebody, Sullivan stratiform

742 sediment-hosted Zn-Pb deposit, British Columbia. Geological Survey of Canada
743 Current Research Paper, 92, 1E, 61-70.
744 London, D. (2011) Experimental synthesis and stability of tourmaline: a historical overview.
745 Canadian Mineralogist, 49, 117-136.
746 London, D. (2013) Crystal-filled cavities in granitic pegmatites: bursting the bubble. Rocks
747 and Minerals 88, 527-534.
748 London, D. (2014a) A petrologic assessment of internal zonation in granitic pegmatites.
749 Lithos 184-187, 74-104.
750 London, D. (2014b) Subsolidus isothermal fractional crystallization. American Mineralogist
751 99, 543-546.
752 Mahood, G., and Hildreth, W. (1983) Large partition coefficients for trace elements in high-
753 silica rhyolites. Geochimica et Cosmochimica Acta, 47, 11-30.
754 Makreski, P., Jovanovski, G., Kaitner, B., Gajović, A., and Biljan, T. (2007) Minerals from
755 Macedonia: XVIII. Vibrational spectra of some sorosilicates. Vibrational
756 spectroscopy, 44, 162-170.
757 McDonough, W.F., and Sun, S.S. (1995) Composition of the Earth. Chemical Geology, 120,
758 223-253.
759 Melleton, J., Gloaguen, E., Frei, D., Novák, M., and Breiter, K. (2012) How are the time of
760 emplacement of rare-element pegmatites, regional metamorphism and magmatism
761 interrelated in the Moldanubian Domain of Variscan Bohemian Massif, Czech
762 Republic? Canadian Mineralogist, 50, 1751-1773.
763 Merlet, C. (1994) An accurate computer correction program for quantitative electron probe
764 microanalysis. Microchimica Acta, 114-115, 1, 363-376.
765 Meyer, R.J. (1911) Über einen skandiumreichen Orthit aus Finnland und den Vorgang seiner
766 Verwitterung. Sitzungsberichte der königlichen preussischen Akademie der
767 Wissenschaften, Berlin 105, 379-384 (in German).
768 Monecke, T., Kempe, U., Monecke, J., Sala, M., and Wolf, D. (2002) Tetrad effect in rare
769 earth element distribution patterns: a method of quantification with application to rock
770 and mineral samples from granite-related rare metal deposits. Geochimica et
771 Cosmochimica Acta, 66, 1185-1196.
772 Morton, A.C., and Hallsworth, C., (2007) Stability of detrital heavy minerals during burial
773 diagenesis. In: Mange, M. A., Wright, D. T. (Eds.), Heavy Minerals In Use.
774 Developments in Sedimentology, 215-245.

775 Morgan, G.B., and London, D. (1989) Experimental reactions of amphibolite with boron-
776 bearing aqueous fluids at 200 MPa: implications for tourmaline stability and partial
777 melting in mafic rocks. Contributions to Mineralogy and Petrology, 102, 281-297.
778 Němec, D. (1990) Neues zur Mineralogie eines Hambergit-führenden Pegmatitigangs von
779 Kracovice (bei Třebíč, Westmorava, ČSFR). Zeitschrift für Geologische
780 Wissenschaften, 18, 1105-1115.
781 Novák, M. (2000) Compositional pathways of tourmaline evolution during primary
782 (magmatic) crystallization in complex (Li) pegmatites of the Moldanubicum, Czech
783 Republic. Memorie della Societa Italiana di Scienze Naturali a del Museo Civico di
784 Storia Naturale di Milano 30, 45-56.
785 Novák, M., Černý, P., Kimbrough, D.L., Taylor, M.C., and Ercit, T.S. (1998a) U–Pb ages of
786 monazite from granitic pegmatites in the Moldanubian Zone and their geological
787 implications. Acta Universitatis Carolinae, Geologica, 42, 309-310.
788 Novák, M., Burns, P.C., and Morgan, G.B.VI. (1998b) Fluorine variation in hambergite from
789 granitic pegmatites. Canadian Mineralogist, 36, 441-446.
790 Novák, M., Černý, P., and Selway, J.B. (1999) The zinnwaldite-masutomilite-elbaite
791 pegmatite at Kracovice from the Třebíč durbachite massif - a complex pegmatite
792 related to the NYF family. The Eugene E. Foord Memorial Symposium on NYF-type
793 Pegmatites, Denver, Colorado, Canadian Mineralogist, 37, 815-816.
794 Novák, M., Škoda, R., Filip, J., Macek, I., and Vaculovič, T. (2011a) Compositional trends in
795 tourmaline from intragranitic NYF pegmatites of the Třebíč Pluton, Czech Republic:
796 an electron microprobe, Mössbauer and LA–ICP–MS study. Canadian Mineralogist,
797 49, 359-380.
798 Novák, M., Gadas, P., Škoda, R., Beurlen, H., and Moura, O.J.M. (2011b) Compositional
799 variations in primary and secondary tourmaline from the Quintos pegmatite,
800 Borborema pegmatite province, Brazil; redistribution of Cu, Mn, Fe and Zn in
801 secondary tourmaline. Asociación Geológica Argentina, Serie D, Publicación
802 Especial, 14, 149-151.
803 Novák, M., Škoda, R., Gadas, P., Krmíček, L., and Černý, P. (2012) Contrasting origins of the
804 mixed (NYF + LCT) signature in granitic pegmatites, with examples from the
805 Moldanubian Zone, Czech Republic. Canadian Mineralogist, 50, 1077-1094.

Novák, M., Kadlec, T., and Gadas, P. (2013) Geological position, mineral assemblages and contamination of granitic pegmatites in the Moldanubian Zone, Czech Republic; examples from the Vlastějovice region. Journal of Geosciences 58, 21-47.

Pantó, G. (1975) Trace minerals of the granitic rocks of the Valence and Mecsek Mountains. Acta Geologica Academiae Scientiarum Hungaricae, 19, 59-93.

Peretyazhko, I.S., and Savina, E.A. (2010) Tetrad effects in the rare earth element patterns of granitoid rocks as an indicator of fluoride-silicate liquid immiscibility in magmatic systems. Journal of Petrology, 18, 514-543.

Pertoldová, J., Týcová, P., Verner, K., Košuličová, M., Pertold, Z., Košler, J., Konopásek, J., and Pudilová, M. (2009) Metamorphic history of skarns, origin of their protolith and implications for genetic interpretation; an example from three units of the Bohemian Massif. Journal of Geosciences, 54, 101-134.

Pesquera, A., Torres-Ruiz, J., Gil-Crespo, P.P., and Jiang, S.-Y. (2005) Petrographic, chemical and B-isotopic insights into the origin of tourmaline-rich rocks and boron recycling in the Martinamor Antiform (Central Iberian Zone, Salamanca, Spain). Journal of Petrology, 46, 1013-1044.

Peterson, R.C., and MacFarlane, D.B. (1993) The rare-earth-element chemistry of allanite from the Grenville province. Canadian Mineralogist, 31, 159-166.

Prokop, J., Losos, Z., Čopjaková, R., and Karásek, J. (2013) Mineralogy and genesis of rock fragments with pegmatite texture from serpentinite eluvium at Nová Ves near Oslavany. Bulletin mineralogicko-petrologického oddělení Národního muzea v Praze, 21, 2, 210-222 (in Czech with English Summary).

Quensel, P. (1945) Berylliumorthit (muromontite) från Skuleboda fältspatbrott. Arkiv för Kemi, Mineralogi och Geologi 18A (22), 1-17 (in Swedish).

Raith, J.G., Riemer, N., Schöner, N., and Meisel, T. (2004) Boron metasomatism and behavior of rare earth elements during formation of tourmaline rocks in the eastern Arunta Inlier, central Australia. Contribution to Mineralogy and Petrology, 147, 91-109.

Roda, E., Pesquera, A., and Velasco, F. (1995) Tourmaline in granitic pegmatites and their country rocks, Fregeneda area, Salamanca, Spain. Canadian Mineralogist, 33, 835-848.

Shannon, R.D. (1976) Revised effective ionic radii and systematic studies of interatomic distances in halides and chalcogenides. Acta Crystallographica Section A: Crystal Physics, Diffraction, Theoretical and General Crystallography, 32, 751-767.

Škoda, R., and Novák, M. (2007) Y,REE,Nb,Ta,Ti-oxide (AB_2O_6) minerals from REL–REE euxenite-subtype pegmatites of the Třebíč Pluton, Czech Republic; substitutions and fractionation trends. Lithos, 95, 43-57.

Škoda, R., Novák, M., and Houzar, S. (2006) Granitic NYF pegmatites of the Třebíč Pluton. Acta Musei Moraviae Scientiae geologicae, 91, 129-176 (in Czech with English Summary).

Škoda, R., Cempírek, J., Filip, J., Novák, M., Veselovský, F., and Čtvrtlík, R. (2012) Allanite-(Nd), $CaNdAl_2Fe_{2+}(SiO_4)(Si_2O_7)O(OH)$, a new mineral from Åskagen, Sweden. American Mineralogist, 97, 983-988.

Slack, J.F., and Robinson, G.R.Jr. (1990) Retrograde metamorphic breakdown of tourmaline at Broken Hill, Australia. Geological Society of America Abstracts with Programs, 22, A126.

Timmerman, M.J. (2008) Palaeozoic Magmatism. In: McCann, T. (Ed.) The Geology of Central Europe, Precambrian and Palaeozoic, 1. Geological Society, London, 665-748.

Torres-Ruiz, J., Pesquera, A., Gil-Crespo, P.P., and Velilla, N. (2003) Origin and petrogenetic implications of tourmaline-rich rocks in the Sierra Nevada (Betic Cordillera, southeastern Spain). Chemical Geology, 197, 55-86.

van Hinsberg, V.J. (2011) Preliminary experimental data on trace-element partitioning between tourmaline and silicate melt. Canadian Mineralogist, 49, 153-163.

van Marcke de Lummen, G. (1986) Tin-bearing epidote from skarn in the Land's End aureole, Cornwall, England. Canadian Mineralogist, 24, 411-415.

Veksler, I.V., Dorfman, A.M., Kamenetsky, M., Dulski, P., and Dingwell, D.B. (2005) Partitioning of lanthanides and Y between immiscible silicate and fluoride melts, fluorite and cryolite and the origin of the lanthanide tetrad effect in igneous rocks. Geochimica et Cosmochimica Acta, 69, 2847-2868.

Wang, A., Han, J., Guo, L., Yu, J., and Zeng, P. (1994) Database of standard Raman spectra of minerals and related inorganic crystals. Applied spectroscopy, 48, 959-968.

Ward, C.D., McArthur, J.M., and Walsh, J.N. (1992) Rare earth element behaviour during evolution and alteration of the Dartmoor granite, SW England. Journal of Petrology, 33, 785-815.

Whitney, D.L., and Evans, B.W. (2010) Abbreviations for names of rock-forming minerals. American Mineralogist, 95, 185-187.

Wolf, M., and London, D. (1997) Boron in granitic magmas: stability of tourmaline in equilibrium with biotite and cordierite. Contribution to Mineralalogy and Petrology, 130, 72-30.

Wu, Ch.-Z, Liu, S.-H., Gu, L.-X., Zhang, Z.-Z., and Lei, R.-X. (2011) Formation mechanism of the lanthanide tetrad effect for a topaz- and amazonite-bearing leucogranite pluton in eastern Xinjiang, NW China. Journal of Asian Earth Sciences, 42, 903-916.

Table captions

Table 1 Summary of tourmaline-bearing samples including textural-paragenetic units, tourmaline type, replacement products and average Y+REE and Sc contents in TurP1. Relative abundance of tourmaline types and replacement products are marked ( ) - absent; (+) - rare; (++) - common; (+++) - abundant. EGM = REE-bearing epidote-group mineral.

Table 2 Representative EMP analyses of tourmaline. Analyses 1-8 – are representative analyses from core-to-rim profile across a tourmaline from the graphic unit, where TurP1 replacement is accompanied by the assemblage REE-bearing epidote-group mineral + chlorite; analyses 9-15 - represent analyses from core-to-rim profile across a tourmaline from the graphic unit, where TurP1 replacement is not accompanied by the assemblage of REE-bearing epidote-group mineral + chlorite; analyses 16-21 represent analyses from core to rim profile across tourmaline from blocky K-feldspar unit; Analyses 22-23 – are representative analyses of secondary tourmaline replacing magmatic TurP1 from blocky K-feldspar unit; analyses 24-29 represent analyses from core-to-rim profile across tourmaline from albite unit; analysis 30 - represents analysis of secondary tourmaline replacing magmatic TurP1 from albite unit; TurP1 replacement by TurS in blocky K-feldspar and albite units is accompanied by REE-bearing epidote-group mineral + chlorite formation. Note: The variable content of Li, unknown Fe^{2+}/Fe^{3+} ratio and evident substitution of Al or/and B for Si in some tourmalines do not allow reliable calculation of the theoretical H_2O and B_2O_3 contents.

Table 3 Representative LA-ICP-MS analyses of trace elements in tourmaline (in ppm). See Table 2 caption for data description.

Table 4 Representative EMP analyses of the REE-bearing epidote-group mineral from different textural-paragenetic units. * Fe^{2+}/Fe^{3+} ratio was calculated to maintain the mineral formula electro-neutral. § Calculated from ideal stoichiometry.

906

907 **Figure captions**

908 Figure 1 BSE images of tourmaline; a) Al-rich schorl (TurP1) with core (TurP1c) darker in
909 BSE image partly replaced by later fluor-elbaite (TurS) with common quartz inclusions
910 (graphic zone); b) Al-rich schorl (TurP1) overgrown by fluor-schorl to fluor-elbaite (TurP2)
911 (albite unit); (c,d) Al-rich schorl (TurP1) overgrown and partially replaced by fluor-schorl to
912 fluor-elbaite (TurP2 and TurS) (albite unit and blocky unit, respectively). The abbreviations
913 for rock-forming minerals are after Whitney and Evans (2010).

914

915 Figure 2 Chemical composition of tourmaline; occupancy of the X-site and ratios of cations in
916 the Y+Z sites; left – Al-rich schorl (TurP1 and TurP1c); right – fluor-schorl to fluor-elbaite
917 (TurP2 and TurS).

918

919 Figure 3 Evolution of selected major and trace elements (EMP data - FeO, F, Na_2O and LA-
920 ICP-MS data – Li, Y+REE, Nd/Nd*) during tourmaline growth; a) albite unit – Al-rich schorl
921 (TurP1) overgrown by later fluor-schorl to fluor-elbaite (TurP2); b) graphic unit; Al-rich
922 schorl with small core TurP1c replaced on the
923 rim by secondary fluor-schorl to fluor-elbaite (TurS); for the b) only: grey line – Al-rich
924 schorl replacement is not accompanied by formation of REE-bearing epidote-group mineral +
925 chlorite; black line – common REE-bearing epidote-group mineral + chlorite form during Al-
926 rich schorl replacement.

927

928 Figure 4 Sc vs. REE contents in tourmaline; a) Al-rich schorl (TurP1c and TurP1); b) fluor-
929 schorl to fluor-elbaite (TurP2 and TurS).

930

931 Figure 5 Chondrite-normalized Y+REE patterns of (a-c) tourmaline and (d) REE-bearing
932 epidote-group mineral (chondrite values after McDonough and Sun 1995). The patterns of the
933 REE-bearing epidote-group mineral combine the EMP and LA-ICP-MS data.

934

935 Figure 6 BSE images of REE-bearing epidote-group mineral (EGM) and chamosite (Chl)
936 replacing Al-rich schorl (TurP1); a-e) graphic unit; f) albite unit.

937

938 Figure 7 Wavelength-dispersive X-ray maps of representative elements for two aggregates of
939 REE-bearing epidote-group mineral.

940

941 Figure 8 Raman spectra of REE-bearing epidote-group mineral compared to the Raman
942 spectra of allanite-(Nd) from Åskagen pegmatite, Sweden.

943

944 Figure 9 Substitution trends of major and minor elements in the REE-bearing epidote-group
945 mineral based on EMP data.

946

947 Figure 10 Ternary plot of major end-members of the epidote group in the REE-bearing
948 epidote-group mineral from the Kracovice pegmatite.

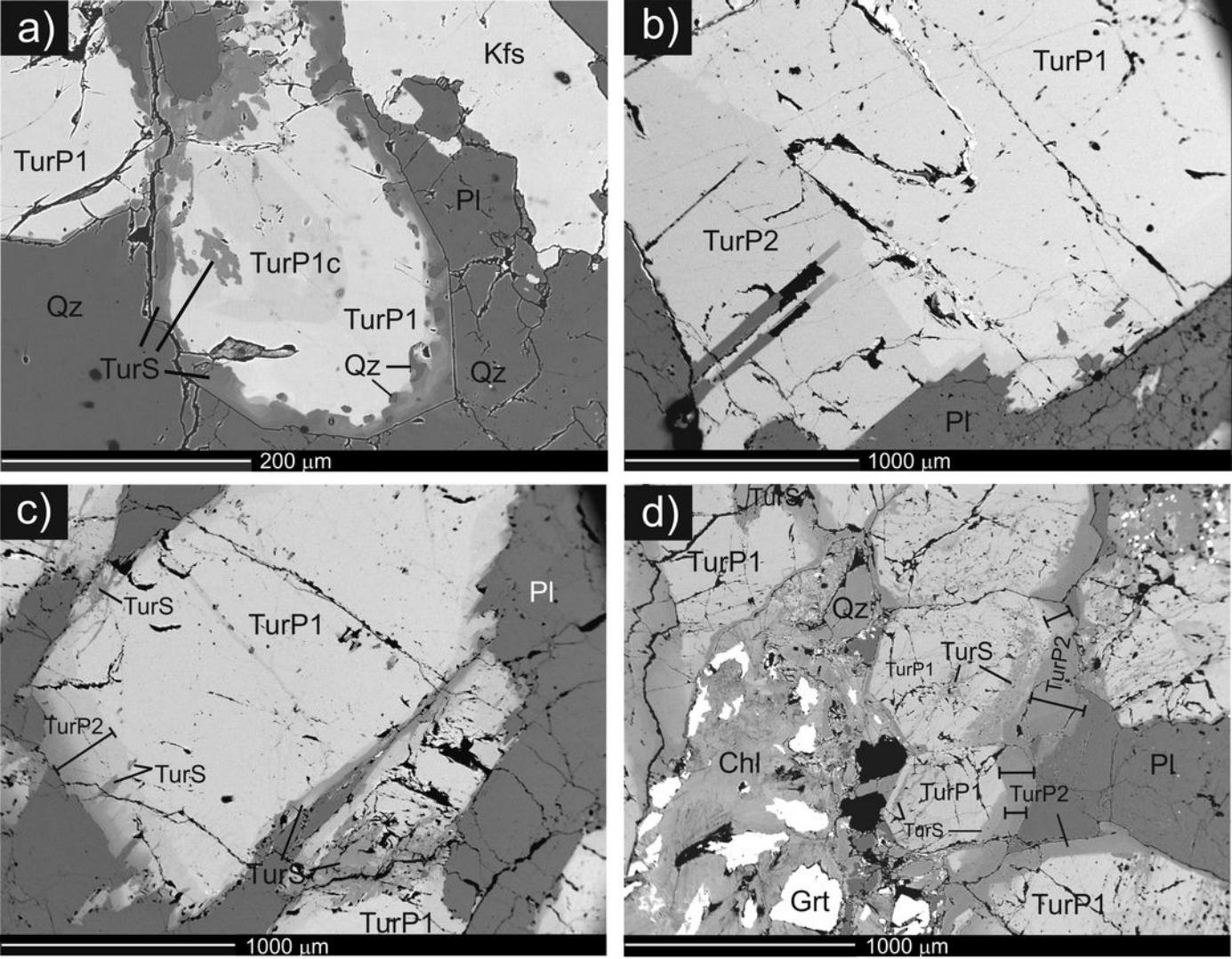
a)
Kfs
TurP1
Pl
TurP1c
Qz
TurP1
TurS
Qz
Qz
200 µm
b)
TurP1
TurP2
Pl
1000 µm
c)
Pl
TurS
TurP1
TurP2
TurS
TurS
TurP1
1000 µm
d)
TurS
TurP1
Qz
TurS
TurP1
TurP2
Chl
Pl
TurP1
TurP2
TurS
Grt
TurP1
1000 µm

Figure 1

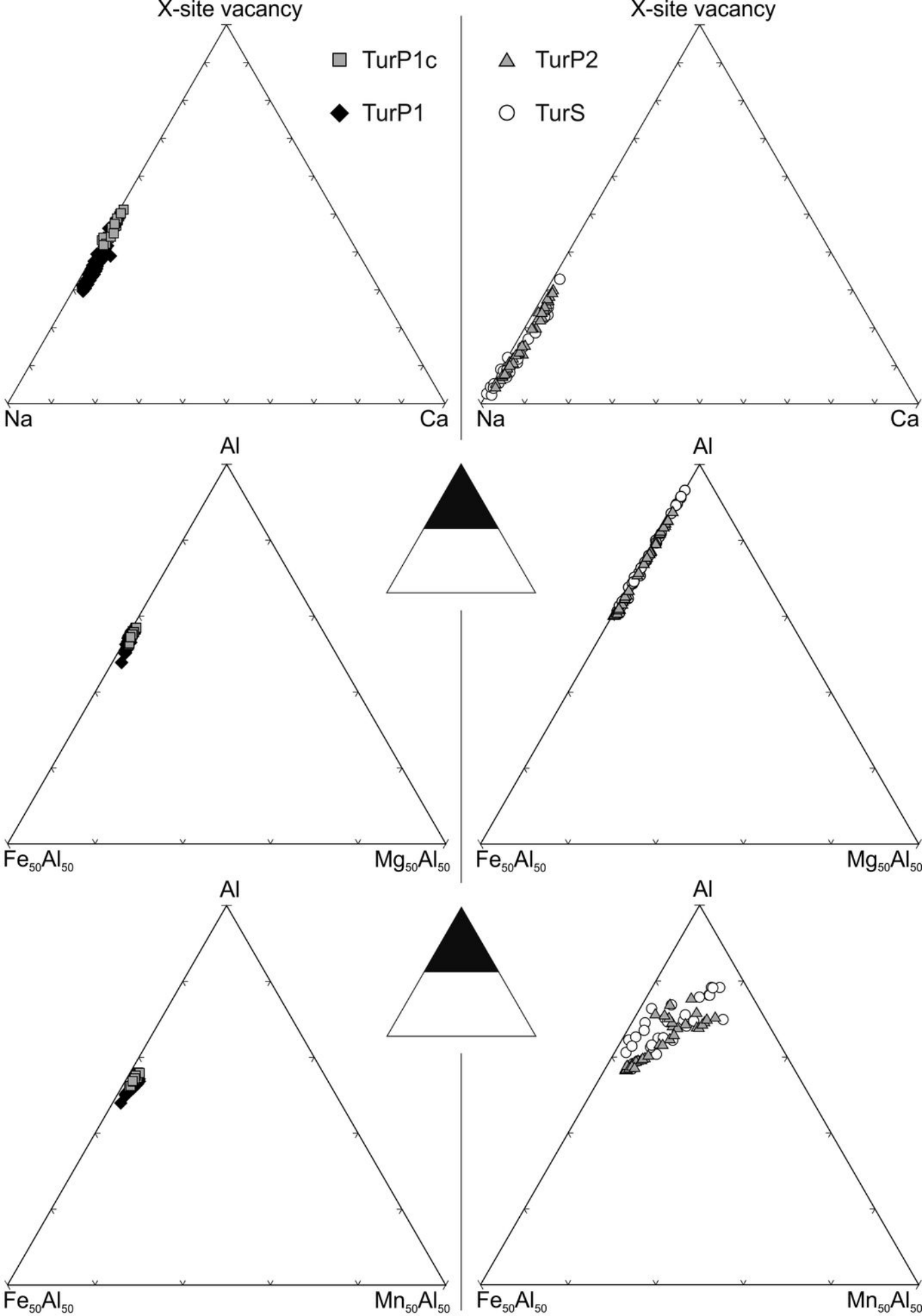
X-site vacancy
TurP1c
TurP1
Na
Ca
X-site vacancy
TurP2
TurS
Na
Ca
Al
Fe50Al50
Mg50Al50
Al
Fe50Al50
Mg50Al50
Al
Fe50Al50
Mn50Al50
Al
Fe50Al50
Mn50Al50

Figure 2

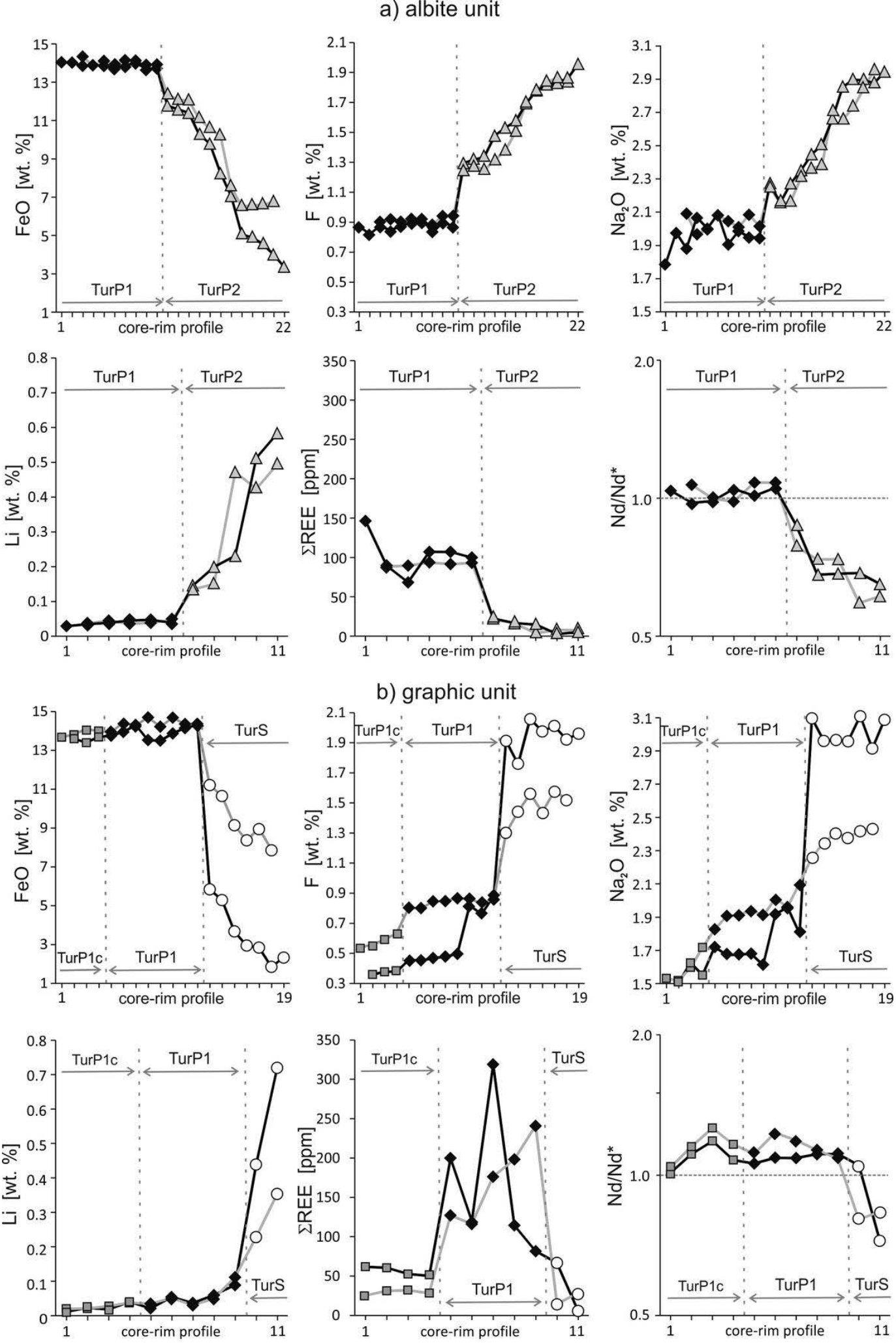
a) albite unit
FeO [wt. %]
F [wt. %]
Na2O [wt. %]
Li [wt. %]
ΣREE [ppm]
Nd/Nd*
TurP1
TurP2
core-rim profile
b) graphic unit
TurP1c
TurS

Figure 3

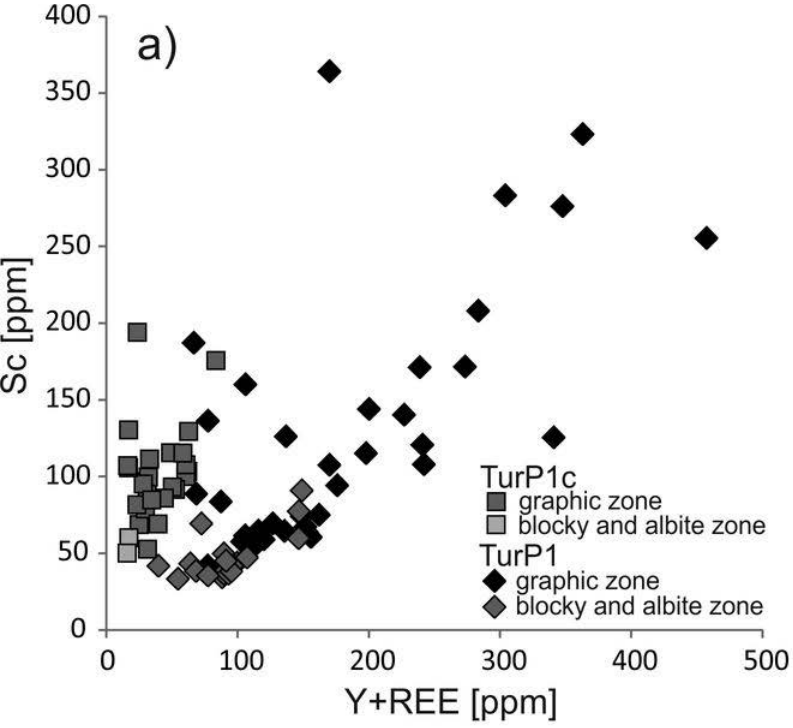
a)
Sc [ppm]
Y+REE [ppm]
0
50
100
150
200
250
300
350
400
0
100
200
300
400
500
TurP1c
graphic zone
blocky and albite zone
TurP1
graphic zone
blocky and albite zone

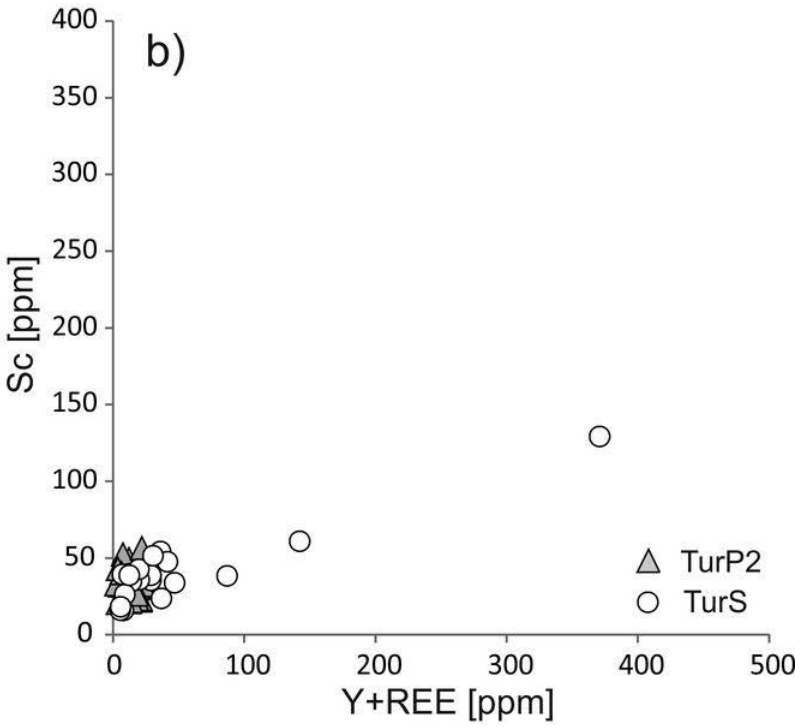
b)
Sc [ppm]
Y+REE [ppm]
0
50
100
150
200
250
300
350
400
0
100
200
300
400
500
TurP2
TurS

Figure 4

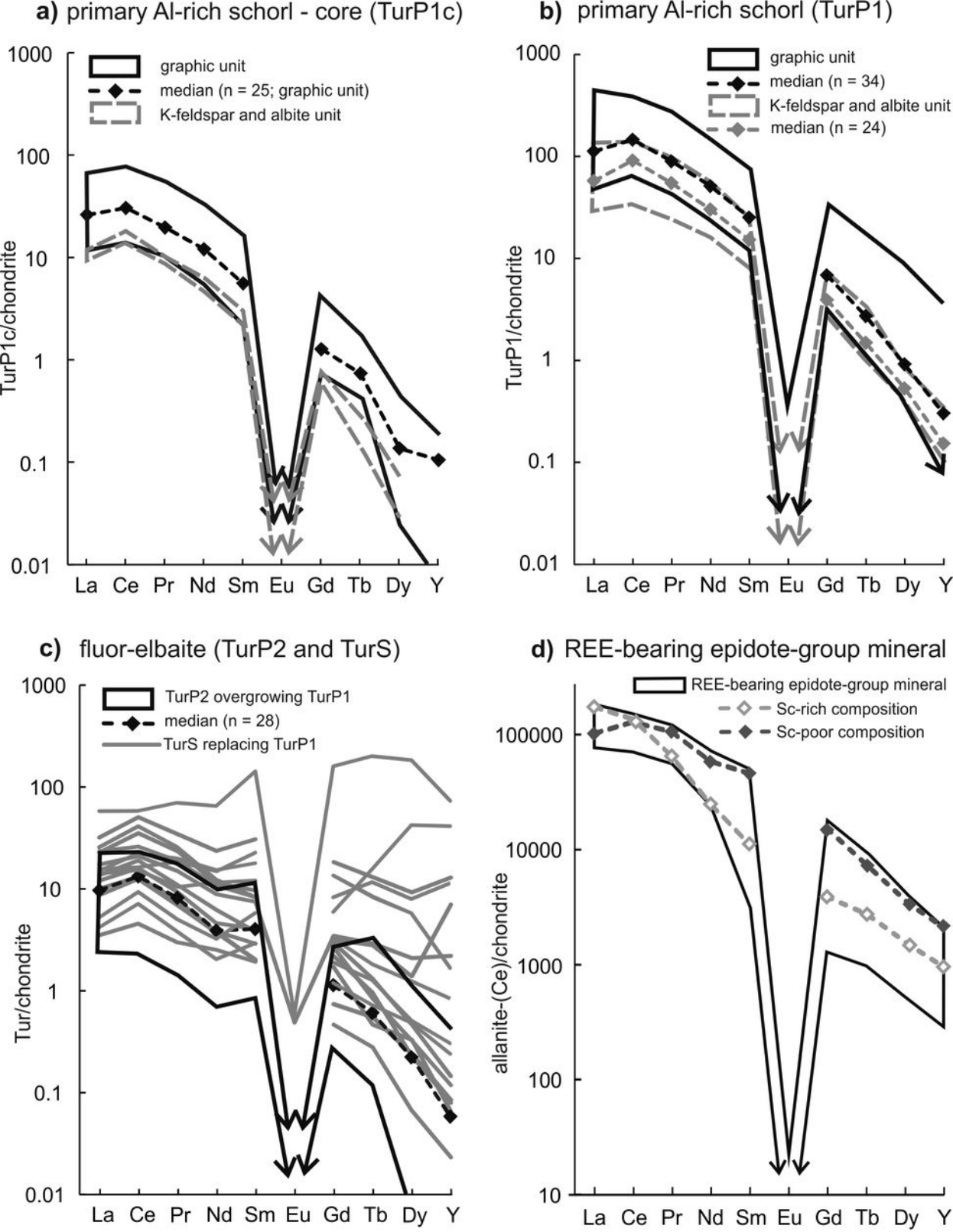
a) primary Al-rich schorl - core (TurP1c)
graphic unit
median (n = 25; graphic unit)
K-feldspar and albite unit
TurP1c/chondrite
1000
100
10
1
0.1
0.01
La Ce Pr Nd Sm Eu Gd Tb Dy Y
b) primary Al-rich schorl (TurP1)
graphic unit
median (n = 34)
K-feldspar and albite unit
median (n = 24)
TurP1/chondrite
1000
100
10
1
0.1
0.01
La Ce Pr Nd Sm Eu Gd Tb Dy Y
c) fluor-elbaite (TurP2 and TurS)
TurP2 overgrowing TurP1
median (n = 28)
TurS replacing TurP1
Tur/chondrite
1000
100
10
1
0.1
0.01
La Ce Pr Nd Sm Eu Gd Tb Dy Y
d) REE-bearing epidote-group mineral
REE-bearing epidote-group mineral
Sc-rich composition
Sc-poor composition
allanite-(Ce)/chondrite
100000
10000
1000
100
10
La Ce Pr Nd Sm Eu Gd Tb Dy Y

Figure 5

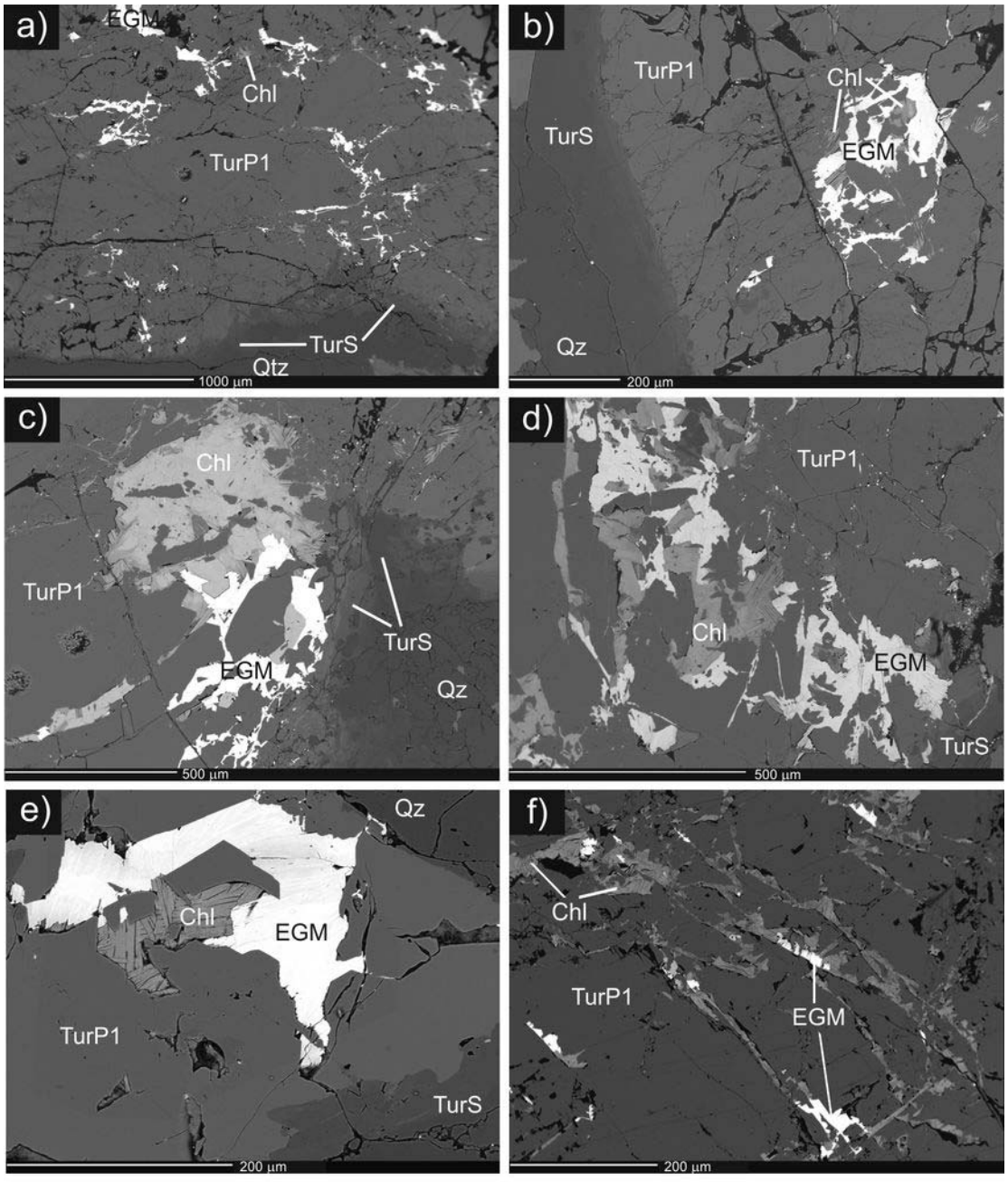
a)
EGM
Chl
TurP1
TurS
Qtz
1000 µm
b)
TurP1
Chl
TurS
EGM
Qz
200 µm
c)
Chl
TurP1
TurS
EGM
Qz
500 µm
d)
TurP1
Chl
EGM
TurS
500 µm
e)
Qz
Chl
EGM
TurP1
TurS
200 µm
f)
Chl
TurP1
EGM
200 µm

Figure 6

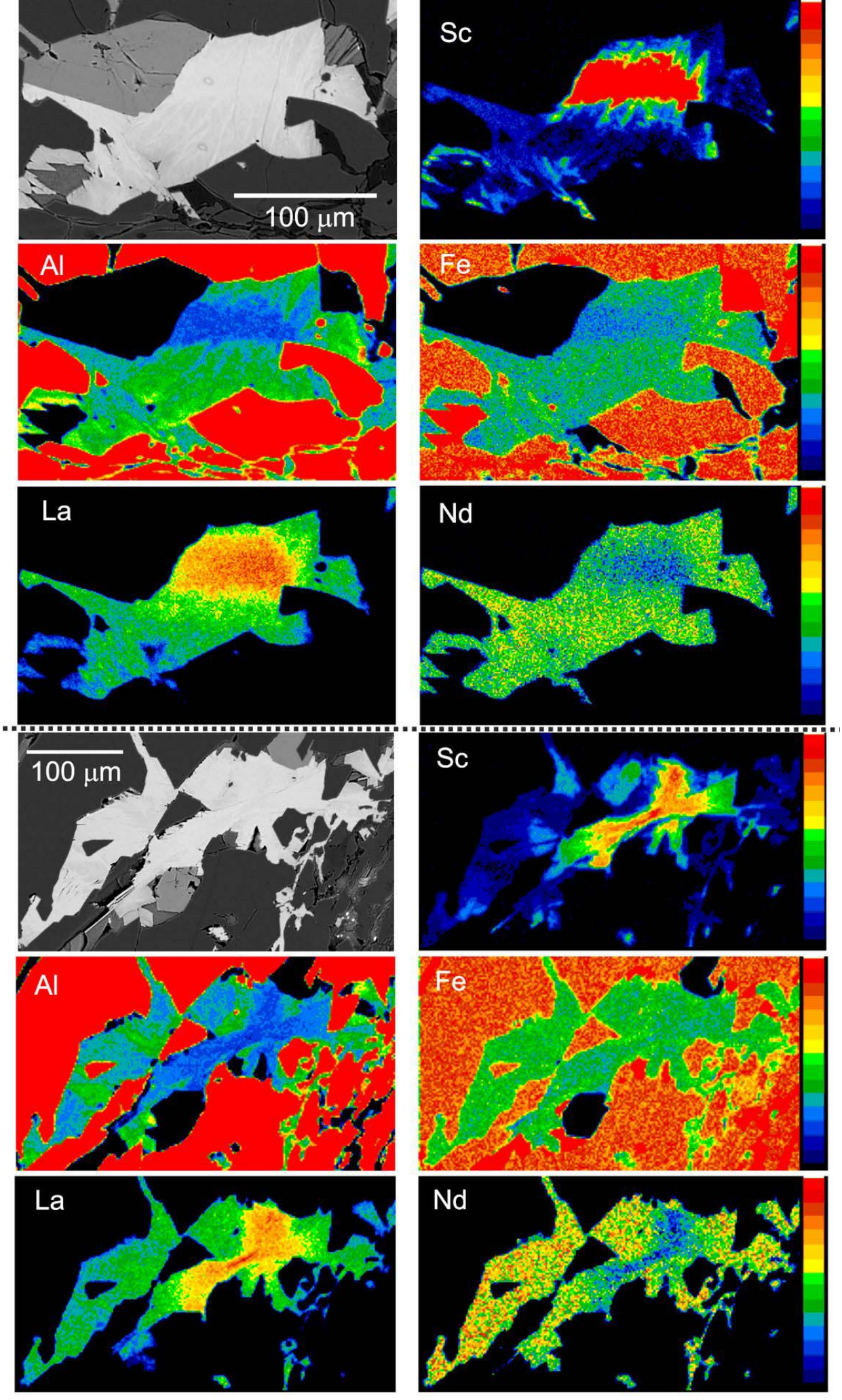

Figure 7

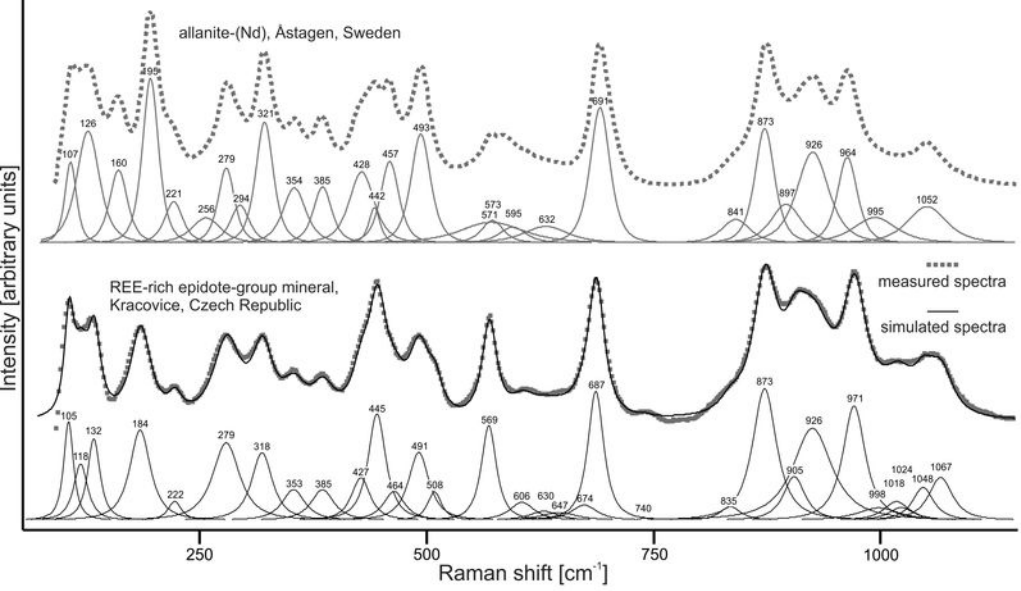
allanite-(Nd), Åstagen, Sweden
107
126
160
221
256
279
294
321
354
385
428
442
457
493
495
573
571
595
632
691
841
873
897
926
964
995
1052
REE-rich epidote-group mineral,
Kracovice, Czech Republic
measured spectra
simulated spectra
105
118
132
184
222
279
318
353
385
427
445
464
491
508
569
606
630
647
674
687
740
835
873
905
926
971
998
1018
1024
1048
1067
Intensity [arbitrary units]
250
500
750
1000
Raman shift [cm-1]

Figure 8

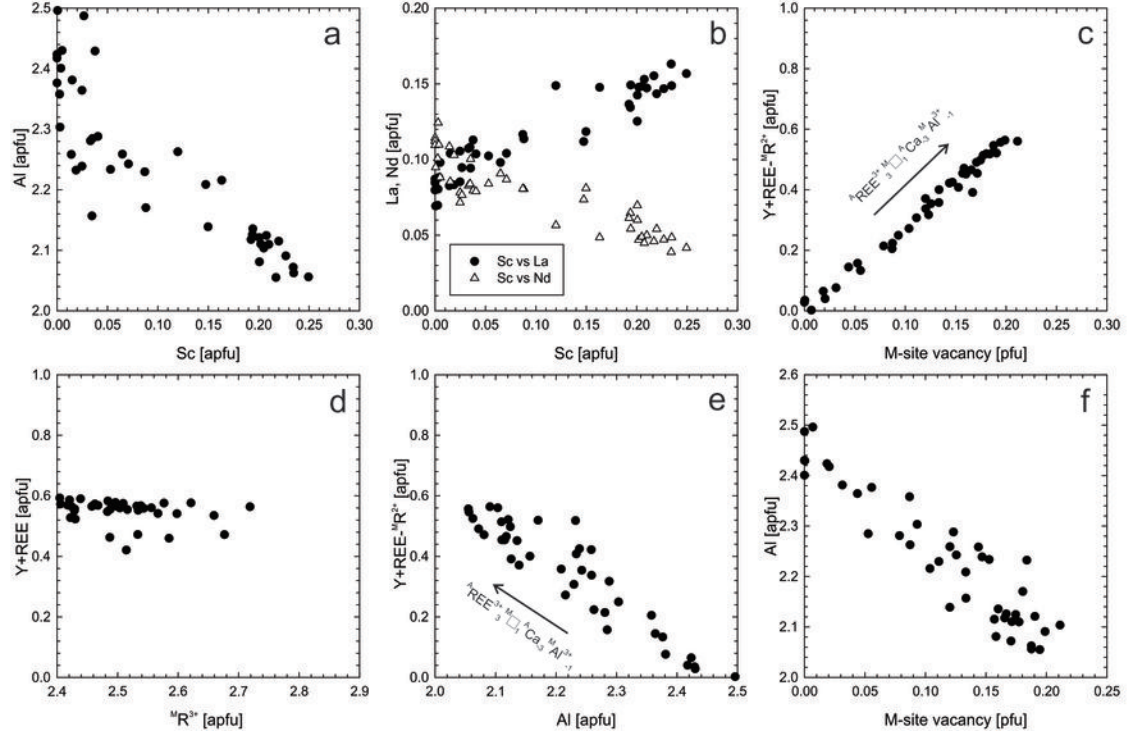
a
Al [apfu]
Sc [apfu]
b
La, Nd [apfu]
Sc [apfu]
Sc vs La
Sc vs Nd
c
Y+REE-$^{M}R^{2+}$ [apfu]
M-site vacancy [pfu]
$^{A}REE^{3+}{}_{3}{}^{M}\square_{1}{}^{A}Ca_{3}{}^{M}Al^{3+}{}_{-1}$
d
Y+REE [apfu]
$^{M}R^{3+}$ [apfu]
e
Y+REE-$^{M}R^{2+}$ [apfu]
Al [apfu]
$^{A}REE^{3+}{}_{3}{}^{M}\square_{1}{}^{A}Ca_{3}{}^{M}Al^{3+}{}_{-1}$
f
Al [apfu]
M-site vacancy [pfu]

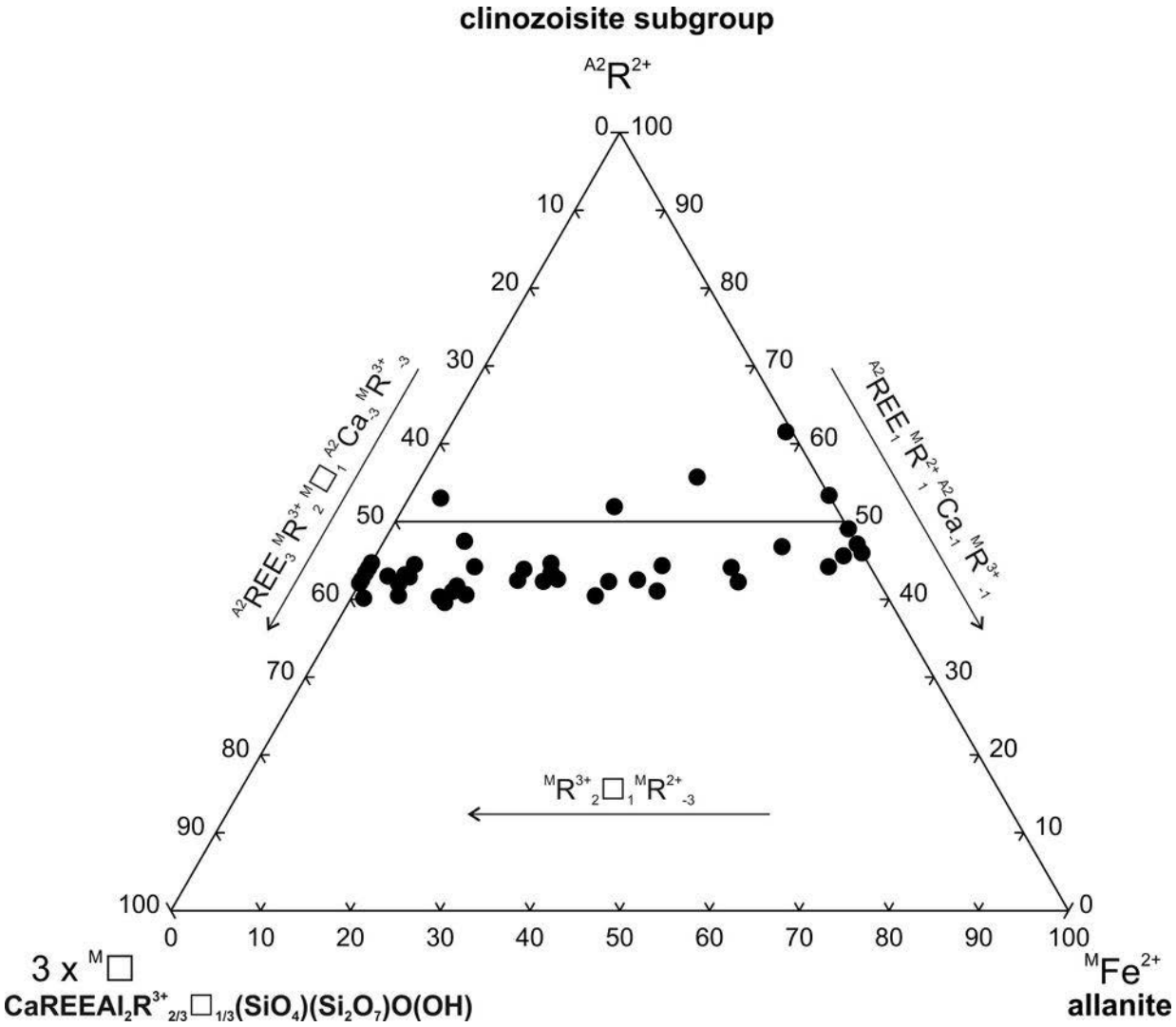
clinozoisite subgroup
$^{A2}R^{2+}$
$^{A2}REE_3{}^{M}R^{3+}{}_2{}^{M}\square_1{}^{A2}Ca_{-3}{}^{M}R^{3+}{}_{-3}$
$^{A2}REE_1{}^{M}R^{2+}{}_1{}^{A2}Ca_{-1}{}^{M}R^{3+}{}_{-1}$
$^{M}R^{3+}{}_2\square_1{}^{M}R^{2+}{}_{-3}$
3 x $^{M}\square$
$CaREEAl_2R^{3+}{}_{2/3}\square_{1/3}(SiO_4)(Si_2O_7)O(OH)$
$^{M}Fe^{2+}$
allanite

	textural-paragenetic unit	TurP1c	TurP1			TurP2	TurS	EGM
		abundance	abundance	REE [ppm]	Sc [ppm]	abundance	abundance	abundance
sample 1	graphic	++	+++	212	238		+++	+++
sample 2	graphic	++	+++	151	82	+	+++	+++
sample 3	graphic/blocky K-feldspar	+	+++	190	113	+++	++	++
sample 4	graphic/blocky K-feldspar	++	+++	161	87		+	
sample 5	blocky K-feldspar		+++	104	48	+++	+	+
sample 6	blocky K-feldspar/albite		+++	95	64	++	+++	++
sample 7	albite unit	+	+++	87	38	+++	++	+

	graphic unit, EGM+Chl formation during TurP1 replacement								graphic unit, without EGM+Chl formation						
	1	2	3	4	5	6	7	8	9	10	11	12	13	14	15
	TurP1c	TurP1c	TurP1	TurP1	TurP1	TurS	TurS	TurS	TurP1c	TurP1c	TurP1	TurP1	TurP1	TurS	TurS
SiO_2	35.67	35.13	34.56	34.71	35.27	36.70	37.53	36.20	34.62	35.29	34.78	34.73	34.85	35.50	35.50
TiO_2	0.04	0.07	0.07	0.15	0.17	0.14	0.09	0.08	0.05	0.08	0.19	0.19	0.21	0.17	0.15
Al_2O_3	35.01	35.33	35.01	33.99	34.15	36.18	37.33	34.18	34.90	34.73	33.75	34.24	34.06	34.65	35.38
MgO	0.14	0.15	0.15	0.19	0.18	0.06	bdl	0.13	0.17	0.14	0.16	0.16	0.14	0.07	0.08
CaO	0.04	0.08	0.06	0.15	0.12	0.15	0.15	bdl	0.03	0.05	0.12	0.12	0.09	0.14	0.19
MnO	0.59	0.66	0.74	0.68	0.68	3.30	4.06	0.78	0.52	0.56	0.66	0.66	0.73	1.96	2.27
FeO	13.68	13.52	13.87	14.14	14.30	5.28	2.33	10.82	13.67	13.99	14.28	14.69	14.68	10.64	8.98
ZnO	0.17	0.32	0.26	0.25	0.31	0.08	bdl	0.20	0.28	0.32	0.41	0.39	0.42	0.36	0.39
Na_2O	1.55	1.68	1.92	1.96	1.80	2.96	3.09	3.02	1.53	1.72	1.91	1.94	2.01	2.35	2.42
K_2O	bdl	0.04	0.05	0.04	0.05	bdl	0.03	0.07	0.03	0.04	0.06	0.04	0.04	0.03	bdl
F	0.38	0.48	0.82	0.76	0.88	1.76	1.96	1.89	0.54	0.64	0.85	0.85	0.86	1.44	1.58
Sum	87.27	87.46	87.50	87.02	87.92	86.60	86.55	87.38	86.34	87.55	87.16	88.02	88.09	87.30	86.93
X-site															
Na^+	0.505	0.548	0.630	0.650	0.591	0.938	0.957	0.970	0.506	0.562	0.633	0.638	0.661	0.769	0.792
Ca^{2+}	0.008	0.015	0.012	0.027	0.022	0.025	0.025	0.000	0.006	0.009	0.022	0.022	0.016	0.026	0.034
K^+	0.000	0.009	0.011	0.009	0.012	0.000	0.006	0.015	0.007	0.009	0.013	0.009	0.010	0.006	0.000
vac	0.487	0.427	0.348	0.315	0.376	0.036	0.012	0.015	0.482	0.420	0.332	0.331	0.314	0.199	0.175
Y,Z site															
Ti^{4+}	0.005	0.009	0.009	0.019	0.021	0.017	0.010	0.010	0.006	0.011	0.025	0.024	0.027	0.021	0.019
Al^{3+}	6.932	6.917	6.849	6.780	6.774	6.972	7.034	6.677	6.895	6.860	6.746	6.712	6.703	6.903	7.049
Fe^{2+}	1.923	1.903	1.965	2.021	2.023	0.722	0.311	1.500	1.946	1.974	2.041	2.080	2.079	1.504	1.269
Mn^{2+}	0.083	0.094	0.107	0.099	0.097	0.457	0.550	0.110	0.076	0.081	0.095	0.095	0.104	0.280	0.325
Mg^{2+}	0.036	0.038	0.037	0.049	0.046	0.014	0.000	0.033	0.042	0.036	0.041	0.041	0.035	0.017	0.019
Zn^{2+}	0.021	0.040	0.033	0.032	0.038	0.010	0.000	0.025	0.036	0.039	0.051	0.048	0.052	0.045	0.049

subtotal	9.000	9.000	9.000	9.000	9.000	8.192	7.905	8.354	9.000	9.000	9.000	9.000	9.000	8.770	8.730
T-site															
Si^{4+}	5.995	5.911	5.857	5.933	5.967	6.000	6.000	6.000	5.893	5.954	5.946	5.880	5.903	6.000	6.000
Al^{3+}	0.005	0.089	0.143	0.067	0.033	0.000	0.000	0.000	0.107	0.046	0.054	0.120	0.097	0.000	0.000
W-site															
F^-	0.201	0.254	0.439	0.411	0.472	0.909	0.991	0.992	0.291	0.339	0.457	0.453	0.462	0.770	0.844
T+Y+Z site	15.000	15.000	15.000	15.000	15.000	14.192	13.905	14.354	15.000	15.000	15.000	15.000	15.000	14.770	14.730
	blocky K-feldspar, EGM+Chl formation								albite unit, EGM+Chl formation						
	16	17	18	19	20	21	22	23	24	25	26	27	28	29	30
	TurP1	TurP1	TurP1	TurP2	TurP2	TurP2	TurS	TurS	TurP1	TurP1	TurP1	TurP2	TurP2	TurP2	TurS
SiO_2	34.87	34.02	34.61	35.19	35.43	36.12	36.27	36.45	34.39	33.81	34.06	34.96	35.19	36.00	36.50
TiO_2	0.19	0.23	0.21	0.22	0.19	0.16	0.18	0.06	0.23	0.24	0.22	0.22	0.12	0.10	0.19
Al_2O_3	34.09	34.33	34.01	35.76	35.82	35.92	35.28	36.21	34.42	34.85	34.48	34.82	35.92	36.30	36.46
MgO	0.12	0.08	0.07	0.07	0.03	0.03	0.06	bdl	0.07	0.09	0.07	0.08	0.08	0.07	0.07
CaO	0.08	0.09	0.08	0.16	0.07	0.10	0.05	0.05	0.12	0.15	0.15	0.12	0.10	0.13	0.13
MnO	0.76	0.80	0.81	2.82	4.62	5.41	3.78	6.06	0.75	0.84	0.86	2.23	3.32	2.36	2.41
FeO	14.02	13.84	14.03	8.52	5.06	3.37	5.60	2.92	14.11	14.15	13.90	10.25	7.54	6.59	6.88
ZnO	0.40	0.36	0.41	0.59	0.24	0.11	0.16	0.13	0.40	0.36	0.41	0.59	0.44	0.23	0.29
Na_2O	1.98	2.00	1.99	2.50	2.86	2.95	3.01	2.91	2.00	2.05	2.08	2.35	2.71	2.84	2.74
K_2O	0.06	0.05	0.04	0.03	bdl	0.05	bdl	0.04	0.05	0.05	0.03	0.06	0.05	0.03	0.04
F	0.82	0.88	0.83	1.63	1.78	1.96	1.87	1.94	0.90	0.89	0.94	1.48	1.69	1.86	1.84
Sum	87.39	86.68	87.07	87.50	86.09	86.18	86.24	86.76	87.44	87.48	87.20	87.15	87.15	86.52	87.54
X-site															
Na^+	0.653	0.667	0.659	0.827	0.937	0.948	0.966	0.928	0.661	0.676	0.692	0.783	0.896	0.919	0.872
Ca^{2+}	0.015	0.017	0.015	0.030	0.013	0.017	0.008	0.008	0.023	0.027	0.027	0.021	0.017	0.022	0.022
K^+	0.012	0.011	0.009	0.007	0.000	0.011	0.000	0.008	0.010	0.011	0.007	0.012	0.011	0.007	0.007
vac	0.319	0.305	0.317	0.136	0.050	0.024	0.025	0.056	0.306	0.286	0.274	0.184	0.076	0.052	0.098
Y,Z site															
Ti^{4+}	0.024	0.029	0.026	0.028	0.024	0.020	0.022	0.007	0.030	0.031	0.028	0.028	0.016	0.012	0.023
Al^{3+}	6.788	6.800	6.780	7.186	7.149	7.032	6.878	7.024	6.782	6.763	6.789	7.043	7.219	7.130	7.064
Fe^{2+}	1.998	1.989	2.007	1.215	0.717	0.468	0.774	0.402	2.012	2.016	1.990	1.471	1.075	0.919	0.946

Mn^{2+}	0.109	0.116	0.117	0.407	0.662	0.762	0.530	0.845	0.108	0.121	0.125	0.324	0.480	0.334	0.336
Mg^{2+}	0.029	0.020	0.018	0.019	0.006	0.008	0.014	0.000	0.018	0.023	0.017	0.019	0.019	0.017	0.018
Zn^{2+}	0.051	0.046	0.052	0.074	0.029	0.013	0.019	0.015	0.051	0.045	0.051	0.074	0.055	0.028	0.035
subtotal	9.000	9.000	9.000	8.930	8.588	8.303	8.237	8.293	9.000	9.000	9.000	8.960	8.864	8.440	8.423
T-site															
Si^{4+}	5.942	5.847	5.922	6.000	6.000	6.000	6.000	6.000	5.864	5.763	5.831	6.000	6.000	6.000	6.000
Al^{3+}	0.058	0.153	0.078	0.000	0.000	0.000	0.000	0.000	0.136	0.237	0.169	0.000	0.000	0.000	0.000
W-site															
F^{-}	0.442	0.476	0.449	0.881	0.953	1.000	0.976	1.000	0.483	0.482	0.510	0.802	0.913	0.981	0.957
T+Y+Z site	15.000	15.000	15.000	14.930	14.588	14.303	14.237	14.293	15.000	15.000	15.000	14.960	14.864	14.440	14.423

peg. unit	graphic unit, EGM+Chl formation during TurP1 replacement									graphic unit, without EGM+Chl formation						
	1	2	3	4	5	6	7	8	9	10	11	12	13	14	15	16
Tur type	TurP1c	TurP1c	TurP1	TurP1	TurP1	TurP1	TurP1	TurS	TurS	TurP1c	TurP1c	TurP1	TurP1	TurP1	TurS	TurS
Li	115	226	209	368	541	594	541	4389	7193	196	378	297	494	1112	2278	3534
Sc	103	100	144	255	323	276	59	38	16	69	95	94	115	121	35	35
Y	0.20	0.25	0.46	3.22	1.49	1.31	0.28	20.30	0.04	0.09	0.12	0.39	0.52	0.60	0.10	3.47
La	10.4	10.3	32.0	105.6	75.2	76.5	20.5	7.6	0.8	4.8	5.5	33.4	36.3	56.8	2.4	4.1
Ce	35.3	34.8	114.1	238.1	184.3	182.9	66.3	31.1	2.8	14.0	14.7	95.4	106.6	130.8	8.0	12.8
Pr	3.69	3.51	12.86	25.41	23.41	19.89	7.42	3.21	0.28	1.42	1.80	11.20	13.25	12.42	0.72	1.39
Nd	9.87	9.66	33.07	63.81	65.08	53.69	20.86	10.77	1.15	3.89	5.19	30.32	34.80	33.21	1.74	4.05
Sm	1.69	1.42	4.99	10.78	9.27	9.67	3.25	4.54	0.29	0.65	0.73	3.83	4.71	4.96	0.43	1.11
Eu	bdl	bdl	bdl	0.02	bdl	bdl	bdl	bdl	bdl	bdl	bdl	bdl	bdl	bdl	0.18	0.03
Gd	0.65	0.63	2.24	6.73	3.15	2.85	1.20	3.65	0.09	0.14	0.25	1.27	1.56	2.05	0.34	0.69
Tb	0.05	0.05	0.20	0.66	0.25	0.18	0.07	0.47	0.01	0.03	bdl	0.09	0.11	0.15	0.02	0.11
Dy	0.05	bdl	0.32	2.28	0.64	0.47	0.16	2.28	0.02	bdl	bdl	0.22	0.16	0.19	0.08	0.51
Er	bdl	bdl	bdl	0.53	0.15	0.13	bdl	1.18	bdl	bdl	bdl	0.08	bdl	bdl	bdl	0.32
Yb	0.05	0.10	0.08	0.42	0.25	0.18	0.08	1.50	bdl	bdl	bdl	bdl	bdl	bdl	bdl	0.30
Lu	0.02	0.04	0.02	0.07	0.06	0.04	bdl	0.23	bdl	bdl	bdl	bdl	bdl	bdl	bdl	0.04
ΣY+REE	62	61	200	458	363	348	120	87	6	25	28	176	198	241	14	29
La_N/Gd_N	13.55	13.60	11.96	13.18	20.06	22.59	14.32	1.75	7.52	27.72	18.50	22.03	19.59	23.30	5.87	5.00
Nd/Nd*	1.01	1.11	1.06	0.99	1.13	0.99	1.09	1.05	0.72	1.04	1.16	1.19	1.13	1.08	0.80	0.84

peg. unit	blocky K-feldspar, EGM+Chl formation							albite unit, EGM+Chl formation							detection	
	17	18	19	20	21	22	23	24	25	26	27	28	29	30	limit	
Tur type	TurP1	TurP1	TurP1	TurP2	TurP2	TurP2	TurS	TurP1	TurP1	TurP1	TurP2	TurP2	TurP2	TurS		
Li	288	449	381	1458	2308	5834	4931	362	446	467	1498	4716	4940	4237	Li	6
Sc	60	47	44	31	26	37	54	34	37	37	23	21	16	21	Sc	0.25
Y	0.24	0.24	0.18	0.09	0.02	0.03	2.61	0.04	0.15	0.11	0.23	0.02	0.38	5.24	Y	0.02
La	24.2	16.8	15.9	3.3	2.1	1.0	3.5	13.2	14.0	12.7	1.9	0.7	1.0	1.0	La	0.02
Ce	87.3	61.9	58.9	12.6	8.1	2.5	13.7	53.4	55.1	55.8	10.6	2.1	4.4	4.0	Ce	0.06
Pr	7.75	6.16	5.71	1.23	0.83	0.28	1.85	4.88	4.70	5.96	0.88	0.19	0.35	0.32	Pr	0.03
Nd	21.76	17.75	15.60	3.73	2.27	0.80	6.96	13.56	12.53	15.43	2.05	0.46	0.93	1.04	Nd	0.06

Sm	3.74	3.07	2.52	0.98	0.88	0.36	2.63	2.17	2.21	2.25	0.58	0.14	0.43	0.64	Sm	0.05
Eu	bdl	bdl	bdl	bdl	bdl	bdl	bdl	bdl	bdl	bdl	bdl	bdl	bdl	bdl	Eu	0.02
Gd	1.38	1.09	0.89	0.42	0.26	0.16	2.68	0.87	0.85	0.77	0.22	0.07	0.24	0.53	Gd	0.04
Tb	0.10	0.08	0.07	0.03	0.03	bdl	0.27	0.06	0.04	0.05	0.03	0.01	0.03	0.04	Tb	0.01
Dy	0.15	0.13	0.10	0.06	0.06	0.05	1.41	0.19	0.08	0.12	0.05	0.04	0.12	0.26	Dy	0.02
Er	bdl	bdl	bdl	bdl	bdl	bdl	0.35	bdl	bdl	bdl	bdl	bdl	bdl	0.11	Er	0.04
Yb	bdl	bdl	bdl	bdl	bdl	bdl	0.25	bdl	bdl	bdl	bdl	bdl	bdl	0.08	Yb	0.04
Lu	bdl	bdl	bdl	bdl	bdl	bdl	bdl	bdl	bdl	bdl	bdl	bdl	bdl	bdl	Lu	0.02
ΣY+REE	147	107	100	22	15	5	34	88	90	93	16	4	8	13		
La_N/Gd_N	14.69	12.99	15.01	6.72	6.85	5.02	1.11	12.75	13.91	13.76	7.14	7.93	3.52	1.57		
Nd/Nd*	1.04	1.05	1.05	0.87	0.68	0.65	0.81	1.07	1.00	1.08	0.73	0.74	0.61	0.59		

	textural-paragenetic unit								
	graphic				blocky K-feldspar		albite		
P_2O_5	0.03	0.04	bdl	0.05	0.08	0.13	0.09	bdl	bdl
SiO_2	33.99	33.89	33.89	34.48	33.94	33.59	33.12	34.12	34.73
TiO_2	0.09	0.03	0.20	0.19	0.05	0.03	0.03	0.06	bdl
ZrO_2	0.52	0.47	0.22	0.06	bdl	bdl	0.03	0.04	0.00
SnO_2	0.69	0.53	0.89	1.05	0.20	0.08	0.41	0.52	0.16
Al_2O_3	19.84	19.71	20.80	21.86	22.86	23.05	21.45	21.54	24.52
Sc_2O_3	3.05	2.82	1.14	0.33	bdl	bdl	0.45	0.25	0.01
Fe_2O_3*	5.95	6.74	6.10	6.69	1.37	0.00	1.76	7.35	0.28
Y_2O_3	0.14	0.22	0.10	0.11	0.14	0.13	0.43	0.22	0.20
La_2O_3	4.57	4.76	3.48	2.66	2.60	2.65	2.83	2.57	2.17
Ce_2O_3	10.18	9.75	10.20	8.11	9.29	9.38	9.21	9.07	6.09
Pr_2O_3	0.91	0.79	1.20	0.99	1.33	1.17	1.15	1.28	0.80
Nd_2O_3	1.54	1.46	2.55	2.52	3.63	3.44	3.11	3.28	3.08
Sm_2O_3	0.06	0.12	0.22	0.36	0.53	0.58	0.79	0.87	0.68
Gd_2O_3	0.05	0.10	0.04	0.10	0.13	0.16	0.34	0.27	0.32
MgO	bdl	bdl	bdl	bdl	bdl	bdl	0.02	bdl	bdl
CaO	14.21	13.98	14.68	16.29	14.41	13.94	13.56	14.20	16.34
MnO	1.07	1.38	0.80	0.71	1.05	1.26	1.31	1.02	1.11
FeO*	0.54	0.04	0.77	0.64	5.90	7.11	5.77	0.62	5.79
SrO	0.78	1.05	0.31	0.26	0.43	0.69	0.89	0.62	0.80
BaO	0.15	bdl	bdl	bdl	bdl	bdl	bdl	bdl	bdl
Na_2O	bdl	0.02	bdl	0.02	0.05	0.04	bdl	bdl	0.02
F	bdl	0.05	0.05	0.04	0.14	0.17	0.10	0.07	0.23
Cl	bdl	0.03	bdl	bdl	bdl	bdl	bdl	bdl	bdl
F,Cl=-O	0.00	-0.03	-0.02	-0.02	-0.06	-0.07	-0.04	-0.03	-0.10
$H_2O^{\S}$	1.70	1.70	1.69	1.72	1.70	1.68	1.66	1.71	1.74
Total	100.06	99.64	99.29	99.21	99.78	99.20	98.44	99.64	98.96
				A-sites					
Na^+		0.004		0.004	0.009	0.006			0.004
Ca^{2+}	1.343	1.324	1.393	1.517	1.362	1.330	1.313	1.338	1.512

Mn^{2+}	0.047	0.059	0.016		0.039	0.060	0.048	0.067	0.024
Sr^{2+}	0.040	0.054	0.016	0.013	0.022	0.035	0.046	0.031	0.040
Ba^{2+}	0.005								
Y^{3+}	0.006	0.011	0.005	0.005	0.006	0.006	0.021	0.010	0.009
La^{3+}	0.149	0.155	0.114	0.085	0.085	0.087	0.094	0.083	0.069
Ce^{3+}	0.329	0.316	0.331	0.258	0.300	0.306	0.305	0.292	0.193
Pr^{3+}	0.029	0.025	0.039	0.031	0.043	0.038	0.038	0.041	0.025
Nd^{3+}	0.049	0.046	0.081	0.078	0.114	0.109	0.100	0.103	0.095
Sm^{3+}	0.002	0.004	0.007	0.011	0.016	0.018	0.025	0.026	0.020
Gd^{3+}	0.001	0.003	0.001	0.003	0.004	0.005	0.010	0.008	0.009
subtot	2.000	2.000	2.000	2.006	2.000	2.000	2.000	2.000	2.000
				M-sites					
Mg^{2+}							0.002		
Mn^{2+}	0.033	0.044	0.044	0.052	0.040	0.035	0.051	0.009	0.057
Fe^{2+}	0.040	0.003	0.057	0.047	0.435	0.529	0.436	0.046	0.419
Al^{3+}	2.062	2.055	2.170	2.239	2.376	2.418	2.285	2.232	2.496
Sc^{3+}	0.235	0.217	0.088	0.025			0.035	0.019	0.001
Fe^{3+}	0.395	0.449	0.406	0.438	0.091		0.120	0.487	0.018
Ti^{4+}	0.006	0.002	0.013	0.012	0.004	0.002	0.002	0.004	
Zr^{4+}	0.022	0.020	0.009	0.002			0.001	0.002	0.000
Sn^{4+}	0.024	0.019	0.031	0.036	0.007	0.003	0.015	0.018	0.006
subtot	2.818	2.809	2.820	2.851	2.953	2.986	2.947	2.816	2.997
				T-sites					
Si^{4+}	2.998	2.997	3.000	2.997	2.994	2.990	2.993	3.000	3.000
P^{5+}	0.002	0.003		0.003	0.006	0.010	0.007		
subtot	3.00	3.00	3.00	3.00	3.00	3.00	3.00	3.00	3.00
F^-		0.015	0.013	0.011	0.040	0.049	0.030	0.018	0.063
Cl^-		0.005							
OH^-	1.000	1.000	1.000	1.000	1.000	1.000	1.000	1.000	1.000
O^{2-}	24.000	23.980	23.987	23.989	23.960	23.951	23.970	23.982	23.937
CZO-EPI	0.44	0.44	0.42	0.53	0.43	0.43	0.41	0.44	0.58
ALL	0.04	0.00	0.06	0.05	0.44	0.53	0.44	0.05	0.42
VAC	0.55	0.56	0.53	0.42	0.11	0.02	0.12	0.53	0.01

Table 4